COPOLYMERS COMPRISING BENZODITHIOPHENE AND BENZOTRIAZOLE DERIVATIVES FOR ORGANIC SOLAR CELLS

A THESIS SUBMITTED TO
THE GRADUATE SCHOOL OF NATURAL AND APPLIED SCIENCES
OF
MIDDLE EAST TECHNICAL UNIVERSITY

BY

DUYGU GÜVEN

IN PARTIAL FULFILLMENT OF THE REQUIREMENTS
FOR
THE DEGREE OF MASTER OF SCIENCE
IN
POLYMER SCIENCE AND TECHNOLOGY

MAY 2016

Approval of the thesis:

COPOLYMERS COMPRISING BENZODITHIOPHENE AND BENZOTRIAZOLE DERIVATIVES FOR ORGANIC SOLAR CELLS

submitted by **DUYGU GÜVEN** in partial fulfillment of the requirements for the degree of **Master of Science in Polymer Science and Technology Department, Middle East Technical University** by,

Prof. Dr. Gülbin Dural Ünver _____
Dean, Graduate School of **Natural and Applied Sciences**

Prof. Dr. Necati Özkan _____
Head of Department, **Polymer Science and Technology**

Assoc. Prof. Dr. Ali Çırpan _____
Supervisor, **Chemistry Department, METU**

Assoc. Prof. Dr. Yasemin Arslan Udum _____
Co-supervisor, **Advanced Technologies Dept., Gazi Uni.**

Examining Committee Members:

Prof. Dr. Levent Toppare _____
Chemistry Dept., METU

Assoc.Prof. Dr. Ali Çırpan _____
Chemistry Dept., METU

Assoc. Prof. Dr. Yasemin Arslan Udum _____
Advanced Technologies Dept., Gazi University

Assoc. Prof. Dr. Dilber Esra Yıldız _____
Physics Dept., Hitit University

Asst. Prof. Dr. Görkem Günbaş _____
Chemistry Dept., METU

Date: 05/05/2016

I hereby declare that all information in this document has been obtained and presented in accordance with academic rules and ethical conduct. I also declare that, as required by these rules and conduct, I have fully cited and referenced all material and results that are not original to this work.

Name, Last name: Duygu Güven

Signature:

ABSTRACT

COPOLYMERS COMPRISING BENZODITHIOPHENE AND BENZOTRIAZOLE DERIVATIVES FOR ORGANIC SOLAR CELLS

Güven, Duygu

M. S., Polymer Science and Technology Department

Supervisor: Assoc.Prof. Dr. Ali Çırpan

Co-Supervisor: Assoc.Prof. Dr. Yasemin Arslan Udum

May 2016, 74 pages

In recent years, converting different energy sources into electricity is under massive investigation. Sun light is an environmental source having a great potential to be utilized as a green energy source. The photovoltaic cells directly convert sun light into electricity. In this study, organic photovoltaic cells in which an active material absorbing sun light and generating electricity were examined. For this aim, two novel organic conjugated polymers were synthesized. Benzodithiophene moiety was used as a donor unit and benzotriazole unit functionalized by alkyl chain was selected as an acceptor unit. Selenophene and thiophene groups were used as π-bridge with their donor character. In this manner, two different conjugated polymers were synthesized via Stille coupling reaction. The electrochromic and photovoltaic properties of the polymers were studied. Average molecular weights of synthesized polymers were calculated by gel permeation chromatography. Cyclic voltammetry was used to investigate redox behaviors and UV-Vis spectrophotometer was used to determine optical properties of polymers. Electronic band gap values of **P-SBTBDTT** and **P-TBTBDTT** were found as 1.96 eV and 2.2 eV, respectively. On the other hand,

optical band gap values were obtained as 1.87 eV and 1.95 eV for **P-SBTBDTT** and **P-TBTBDTT**, sequentially. In photovoltaic studies, device fabrication was carried out in a moisture free glove box. Devices were constructed by using ITO coated glass substrate covered by different ratios of polymer:$PC_{71}BM$ layers. Consequently, the highest power conversion efficiency was found as 1.50 % for **P-TBTBDTT** under standard AM 1.5 G illumination (100 mW/cm^2) in the preliminary studies.

Keywords: Benzotriazole, benzodithiophene, selenophene, conjugated polymers, organic solar cell

ÖZ

ORGANİK GÜNEŞ PİLLERİ İÇİN BENZODİTİYOFEN VE BENZOTRİAZOL TÜREVLERİ İÇEREN KOPOLİMERLER

Güven, Duygu

Yüksek Lisans, Polimer Bilimi ve Teknolojisi Bölümü

Tez Yöneticisi: Doç.Dr. Ali Çırpan

Ortak Tez Yöneticisi: Doç.Dr. Yasemin Arslan Udum

Mayıs 2016, 74 sayfa

Son yıllarda farklı enerji kaynaklarını elektriğe çevirmek için birçok araştırma yapılmaktadır. Güneş ışığı bu çalışmalarda kullanılmak için en yüksek potansiyele sahip olan çevresel bir kaynaktır. Bu çalışmada içinde güneş ışığını absorbe eden aktif malzemesi bulunan ve birkaç etkileşme ile güneş ışığını elektriğe çeviren organik fotovoltaik piller araştırıldı. Bu amaçla, özgün konjuge polimerler sentezlendi. Benzoditiyofen ünitesi donör olarak, alkil zinciri ile fonksiyonlandırılmış benzotriazol ünitesi ise akseptör olarak kullanıldı. Selenofen ve tiyofen grupları donör özellikleri ile π-köprüsü olarak kullanıldı. Bu şekilde, iki farklı konjuge polimer Stille kenetleme reaksiyonu kullanılarak sentezlendi. Polimerlerin elektrokromik ve fotovoltaik özellikleri çalışıldı. Sentezlenen polimerlerin ortalama molekül ağırlıkları jel permeasyon kromatografisi kullanılarak hesaplandı. Polimerlerin redoks davranışları dönüşümlü voltametri kullanılarak yapılırken optik özellikleri UV-Vis spektrofotometre ile belirlendi. **P-SBTBDTT** ve **P-TBTBDTT** polimerlerinin elektronik bant aralıkları 1.96 eV ve 2.2 eV bulundu. Bununla birlikte optik bant aralıkları 1.87 eV ve 1.95 eV hesaplandı. Fotovoltaik çalışmalarda, cihaz yapımı havasız ortam kabini içerisinde gerçekleştirildi. Cihazlar,

ITO kaplı cam yüzeye farklı oranlarda polimer:$PC_{71}BM$ katmanları kaplanarak elde edildi. Sonuç olarak, yapılan ön çalışmalarda en yüksek güç dönüşüm verimi **P-TBTBDTT** için standart AM 1.5 G aydınlatma (100 mW/cm^2) altında 1.50 % olarak elde edildi.

Anahtar Kelimeler: Benzotriazol, benzoditiyofen, selenofen, konjuge polimerler, organik güneş pili

To my precious family

ACKNOWLEDGEMENTS

First and foremost, I would like to express my sincere gratitude to my supervisor Assoc. Prof. Dr. Ali Çırpan for his endless support, guidance, patience and invaluable opportunities that are offered during my thesis study.

I am grateful to Prof. Dr. Levent Toppare for his scientific support, expertise and meritorious contributions to my thesis.

I would like to thank my co-supervisor Assoc. Prof. Dr. Yasemin Arslan Udum for her valuable support and guidance.

I would like to express my gratitude to Asst. Prof. Dr. Görkem Günbaş for his support and contributions to my thesis, especially in organic chemistry field.

I am grateful to Şerife Hacıoğlu and Gönül Hızalan for their valuable guidance and elaboration on electrochemical and photovoltaic studies.

I would like to thank to Şevki Can Cevher for his guidance and support during my thesis study period.

I am grateful to Hande Ünay for her precious friendship, encouragement and guidance. She always stands for me anytime I needed. I also would like to thank to Naime Akbaşoğlu Ünlü for her kind support and guidance.

I would like to express my feelings to Özlem Sever Güngör and Birsu Teoman Kölemen for their friendships, support and motivations.

I sincerely thank İpek, Ece, Özge, Aslı, Soner, Cansel, Duygu, Nima, Janset, Emre, Sultan and Dr. Fatma Demir for their friendships, motivations, support and providing such a peaceful working environment.

I want to offer my special and endless thanks to Arda Güleş for his endless support, understanding and invaluable love. And special thanks to my lovely friends Beril Kapusuz Balcı and Anıl Balcı for their motivations, support and enjoyable conversations.

The last but not the least, I owe a lot to my precious parents for their endless love, guidance and encouragement.

TABLE OF CONTENTS

LIST OF TABLES

TABLES

LIST OF FIGURES

FIGURES

LIST OF SCHEMES

SCHEMES

ABBREVATIONS

HOMO	Highest Occupied Molecular Orbital
LUMO	Lowest Unoccupied Molecular Orbital
VB	Valence Band
CB	Conduction Band
BLA	Bond Length Alternation
D	Donor
A	Acceptor
EC	Electrochromic
OLED	Organic Light Emitting Diode
LED	Light Emitting Diode
OFET	Organic Field Effect Transistor
OPV	Organic Photovoltaics
BTz	Benzo[d][1,2,3]triazole
BDT	Benzo[1,2-b:4,5-b′]dithiophene
PEDOT	Poly(3,4-ethylenedioxythiophene)
PSS	Polystyrene sulfonate
PCBM	[6,6]-Phenyl-C_{61}-butyric acid methyl ester
MPP	Maximum Power Point
PCE	Power Conversion Efficiency
ITO	Indium Tin Oxide
PDI	Polydispersity Index
GPC	Gel Permeation Chromatography
CV	Cyclic Voltammetry
WE	Working Electrode
CE	Counter Electrode
RE	Reference Electrode
$TBAPF_6$	Tetrabutylammoniumhexafluorophosphate
ACN	Acetonitrile

UV	Ultraviolet
Vis	Visible
IR	Infrared
$\boldsymbol{V_{OC}}$	Open Circuit Voltage
$\boldsymbol{I_{SC}}$	Short Circuit Current
$\boldsymbol{J_{SC}}$	Short Circuit Current Density
FF	Fill Factor
$\boldsymbol{P_{in}}$	Incident Light Power Density
THF	Tetrahydrofuran
DCM	Dichloromethane
$\mathbf{E_g^{op}}$	Optical Band Gap
$\mathbf{E_g^{el}}$	Electronic Band Gap

CHAPTER 1

INTRODUCTION

Polymers are macromolecules formed by the repeating units of a large number of small molecules in a regular sequence. Polymers have been widely used due to their flexibility, processability, low cost, environmental stability, light weight, tailorability, etc. Chemical composition, molecular forces, molecular weight distribution and morphology affect the properties of polymers.[1]

1.1. Conjugated Polymers

Conjugated polymers are organic polymers that conduct electricity. They show the electrical, electronic, optical and magnetic properties of metal while keeping the properties of conventional polymer such as mechanical properties, processability, etc.[2] In 2000 Alan J. Heeger, Alan G. MacDiarmid and Hideki Shirakawa were awarded the Nobel prize *"for the discovery and development of conductive polymers"*.[3] That discovery created new research areas in organic electronics and photonics such as light emitting diodes (LEDs),[4] electrochromics, [5] field effect transistors, [6] photovoltaic cells [7] and biosensors.[8]

Intrinsically conducting polymers have conjugated double bonds.[9] π-electron conjugated polymers consist of alternating single and double bonds through the polymer backbone. Some examples of conjugated polymers are; polyacetylane, polypyrrole, polythiophene, polyaniline, polyfuran, etc. Repeating unit structures of some conjugated polymers are illustrated in Figure 1.

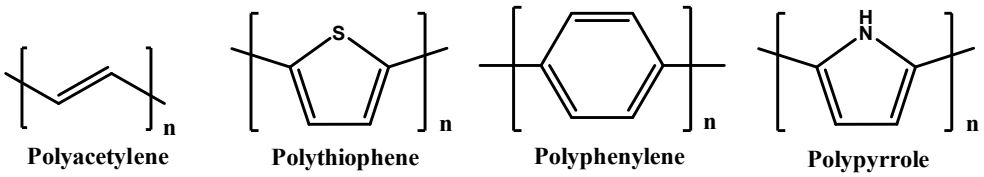

Figure 1. Repeating unit structures of some conjugated polymers

In conjugated polymer, all the atoms are generally sp^2-hybridized throughout the main polymer backbone. While one unhybridized p-orbital in each atom stays perpendicular to the plane of polymer chain, all other p-orbitals are parallel to each other. Therefore, due to lateral overlapping of p-orbitals on either side, p-orbitals are delocalized throughout the polymer chain, as shown in Figure 2.[10] As a result of π-electron delocalization, electron can move from one bond to another enabling the polymer to gain conductivity.[11,12]

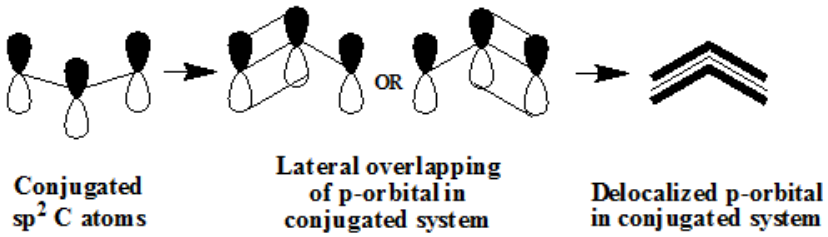

Figure 2. Delocalization of p-orbital in a conjugated carbon chain

1.2. Band Theory

Conductivity of material is directly affected by the band gap value. The energy difference between HOMO (Highest Occupied Molecular Orbital) and LUMO (Lowest Unoccupied Molecular Orbital) energy levels is called as band gap. For polymers, the HOMO is denoted as valence band (VB) and the LUMO is denoted as conduction band (CB). According to electrical conduction, the materials are classified as conductors, semiconductors and insulators. Band gap structures of conductors (metals), semiconductors and insulators are shown in Figure 3.

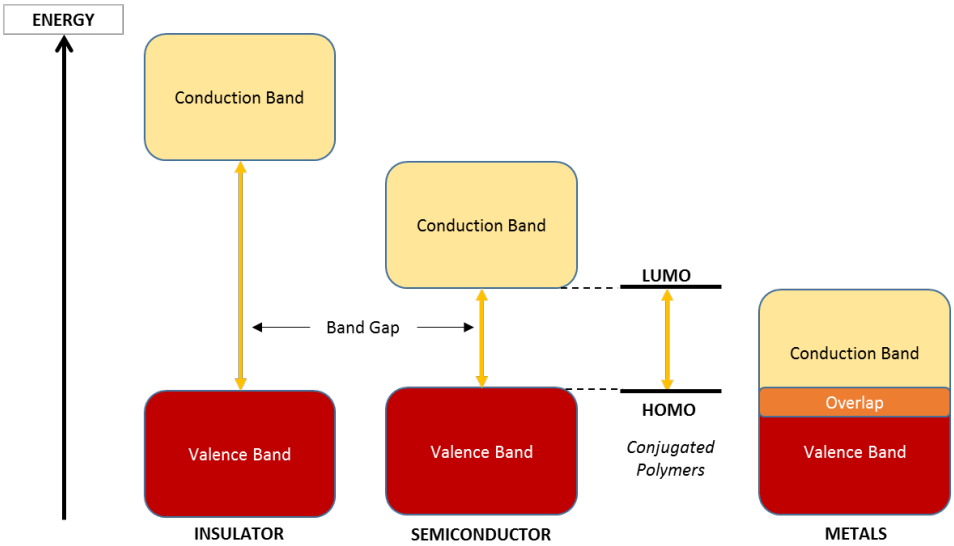

Figure 3. Band gap structures for insulator, semiconductor and conductor

Optical and optoelectronic properties of π-conjugated polymers depend on the difference between HOMO and LUMO energy levels. Structural modifications enable to obtain low band gap polymers. [13]

1.3. Doping Process

For saturated types of polymers, the band gap is higher than 4 eV. They show insulating behavior due to restriction of movement of electrons from the valence band to conduction band.[14] In conjugated polymers, HOMO is increased while the LUMO is decreased based on delocalization through the polymer chain. As a result, neutral stable (undoped) conjugated polymers have high band gap locating in the lower semiconducting region. However, their conductivity is almost similar to that of insulator which is 10^{-7}-10^{-11} S/cm. Therefore, doping process is used as an effective method to convert π-conjugated polymers to electrically conducting polymers.[13]

Doping is the process, used to introduce mobile charge carriers by oxidation or reduction reactions. Changes in the electrical, electronic, magnetic, optical and structural properties of the polymer occur by the controlled addition of chemical species having known small (<10%) nonstoichiometric amounts. The process is defined as p-doping if electrons from the valence band which is HOMO of

conjugated polymer are removed by oxidizing agent. While, the process is denoted as n-doping when an electron is donated by a reducing agent to the empty conduction band which is LUMO of conjugated polymer. Counter anions or cations are used as dopants to neutralize these positive or negative charges, respectively.[15,16]

Electrical conductivity as well as electrochemical and electrochromic properties of polymers are the result of redox reactions. Some examples of these redox reactions in conducting polymers are;

a) chemical doping of polyacetylene

$(CH)_n + nyX \longrightarrow [(CH)^{+y} X_{y-}]_n$ p-type X = Br_2, I_2 …

$(CH)_n + nyM \longrightarrow [(CH)^{-y} X_{y+}]_n$ n-type M = Na, Li …

b) electrochemical doping of polythiophene

$(T)_n + nyX^- \longrightarrow [T^{+y} X_{y-}]_n + nye^-$ p-type X = ClO_4^-

$(T)_n + nyM^+ \longrightarrow [T^{+y} M_{y+}]_n + nye^-$ n-type M = Li^+

Little or no degradation takes place in the polymer chain when the doping process is applied to conducting polymer. Conducting polymers can be used in applications such as rechargeable batteries and electrochromic displays due to the ability of cycling between charged and neutral states.[17]

1.4. Band Gap Engineering

In order to modify the electronic properties of semiconducting polymers, the band gap of the materials can be tuned. Band gap engineering consists of parameters such as bond length alternation (E_{bla}), aromaticity (E_{Res}), planarity (E_{θ}), substituents (E_{Sub}), and intermolecular interactions (E_{int}).[18] Structural factors determining the band gap of polymers are illustrated in Figure 4.

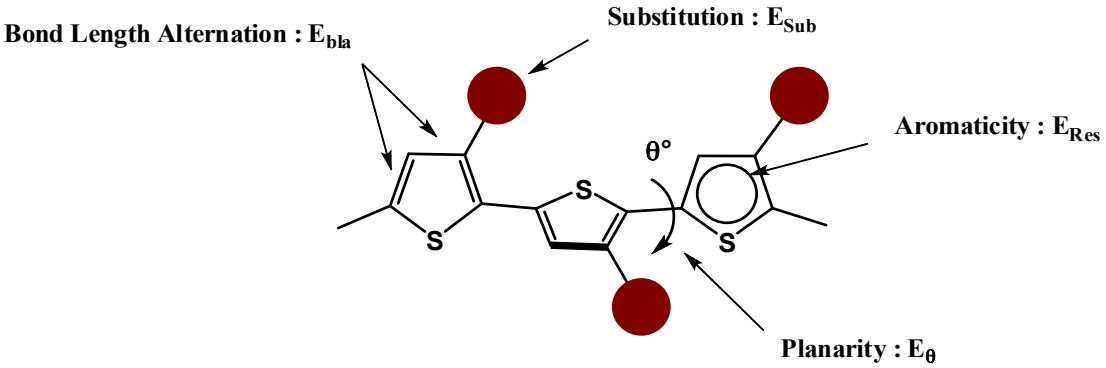

Figure 4. Structural factors determining the band gap of materials derived from linear π-conjugated systems

1.5. Bond Length Alternation

A series of successive carbon-carbon double bonds of polyaromatic conjugated polymers are linked by a carbon-carbon single bond. For their ground state there are two resonance structures with nondegenerate energy, aromatic and quinoid forms. In aromatic form, confined π-electrons provide aromaticity. Resonance structure turns into quinoid form by delocalization of π-electrons along the conjugated chain. The quinoid form is energetically less stable and has a smaller band gap due to destruction of the aromaticity and loss in the stabilization energy. In a polyaromatic conjugated system, the ratio of aromatic to quinoid form is associated with bond length alternation (BLA). Bond length alternation is defined as the average difference in length between two adjacent bonds.[19] In Figure 5 aromatic and quinoid resonance of some polymers are shown.

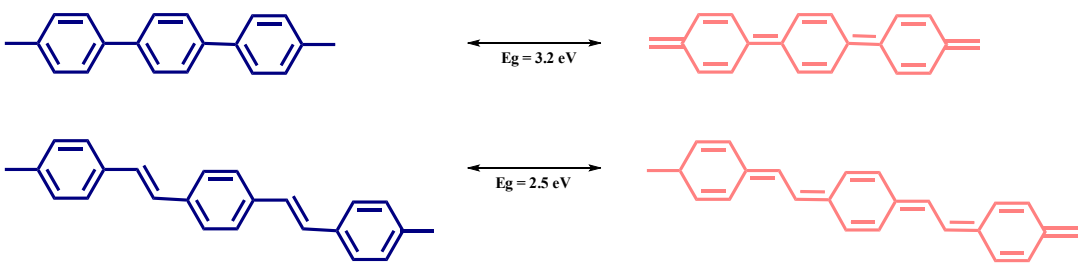

Figure 5. Aromatic and quinoid resonance forms of poly(p-phenylene) and poly(p-phenylenevinylene)

1.5.1. Aromaticity

If aromaticity of the aromatic units decreased in the conjugated main chain, tendency to quinoid form will be greater. Hence, band gap of the molecule decreases due to increase in π-electron delocalization.[20]

1.5.2. Planarity

In order to extend conjugation and enable delocalization, parallel p-orbital interactions are obtained by planarization. As a result, decrease in bond length alternation and reduction in band gap occur.[21]

1.5.3. Substituent Effects

HOMO and LUMO levels of a conjugated system can be modulated by the incorporation of electron-withdrawing or electron-donating substituents. While electron-withdrawing groups lower the LUMO energy, electron-donating substituents increase the HOMO energy, leading decreased band gap.[22]

1.5.4. Intermolecular Interactions

Molecules in solid state have more close-packed and ordered crystalline structure than materials in solution state. In the solid state, intermolecular interactions induced by secondary forces increase interchain delocalization resulting in reduction of band gap.[23]

1.6. Donor-Acceptor Approach

In designing low band gap conjugated polymers, electron-rich donor (D) and electron-deficient acceptor (A) should be incorporated into the polymer backbone.[24] Bond length alternation is decreased by push-pull driving forces enabling electron delocalization and mesomeric structures of quinoid formation. In addition, optical band gap is reduced by high-lying HOMO of donor and low-lying LUMO of acceptor.[25] According to perturbation theory, highest occupied molecular orbitals of donor and acceptor segments interact to yield two new HOMO levels for D-A polymer. In a similar manner, lowest unoccupied molecular orbitals of donor and acceptor form two new LUMO levels of D-A polymer. Higher lying HOMO and lower lying LUMO levels are created after redistribution of electrons from their non-interacting orbitals to the new hybridized orbitals of polymer which is shown in Figure 6.[26]

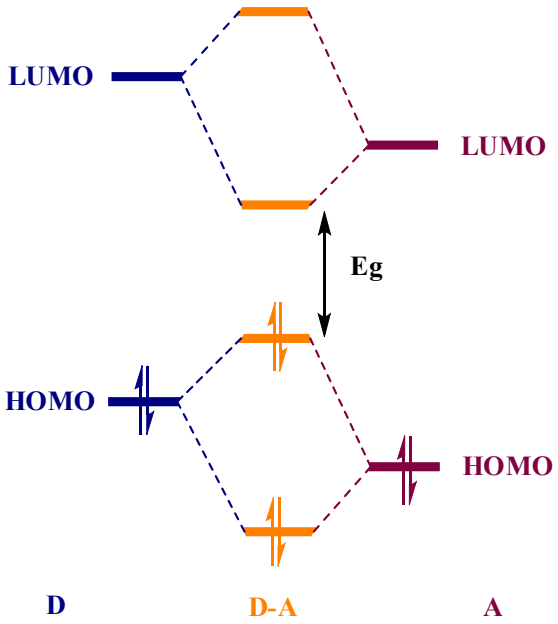

Figure 6. Orbital interactions of donor and acceptor units leading to a smaller band gap in a D-A conjugated polymer

1.7. Synthesis of Conjugated Polymers

Transition-metal-catalyzed cross coupling reactions are widely used in construction of polymers in addition to electrochemical [31-33] or chemical oxidative [34] polymerizations. In general, the reaction starts with transition-metal-catalyzed oxidative addition reaction of an electrophile across the C-X bond followed by transmetallation with a main group organometallic nucleophile. Then, reductive elimination results in carbon-carbon bond formation and active catalyst regeneration.[35] Nickel- or palladium-based complexes are commonly used as transition-metal catalysts. Grignard reagents (Kumada-Corriu),[36] boron reagents (Suzuki-Miyaura),[37] copper (Sonogashira)[38] or stannyl (Stille)[39] can be used as organometallic nucleophiles in coupling reactions. The main advantage of these reactions is occurring in mild conditions.

1.7.1. Palladium-Catalyzed Cross Coupling Reactions

The mechanism of reaction starts with the oxidative addition of an organic halide to the catalyst. Palladium has high functional group tolerance. In addition, organopalladium compounds have low sensitivity towards water and air.[40] Then, transmetallation with another organometallic reagent (nucleophile) takes place. Finally, reductive elimination occurs to regenerate the catalyst and the organic product is obtained.[41] Catalytic cycle of palladium-catalyzed cross coupling reactions is illustrated in Scheme 1.

Scheme 1. Catalytic Cycle of Palladium-Catalyzed Cross Coupling Reactions

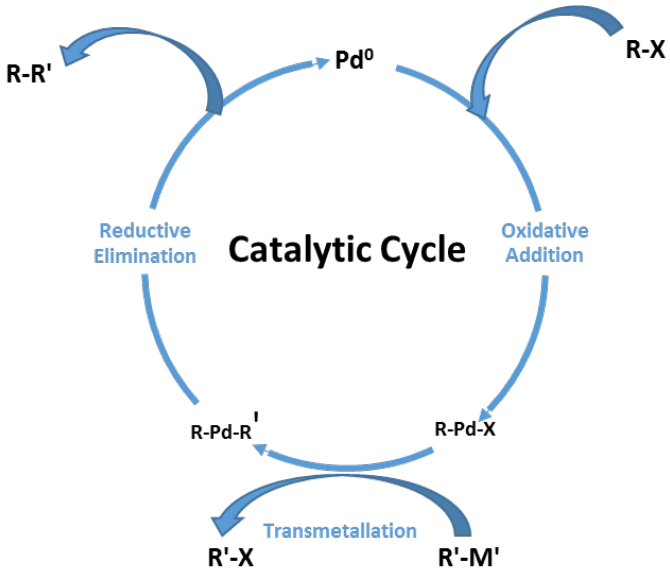

1.8. Moieties in Donor-Acceptor Approach Conjugated Polymers

1.8.1. Benzotriazole Moiety

The first benzotriazole polymer was synthesized by Tanimoto and Yamamoto. Benzotriazole unit has moderately electron-deficient property due to the diimine structure. One of the nitrogen atoms on the triazole unit can be modified with solubilizing alkyl groups. Therefore, benzotriazole can be used to obtain solution processable polymers.[42] Additionally, benzotriazole-based polymers have been widely used in applications such as electrochromics [43], OFET [44], OPV [45] and OLED [46]. Structure of benzotriazole is shown in Figure 7.

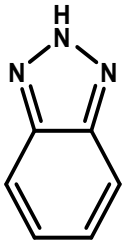

Figure 7. Structure of Benzotriazole

1.8.2. π-Bridge Groups: Thiophene and Selenophene

Thiophene containing polymers are used as electron donors in bulk heterojunction organic photovoltaics due to their π-conjugated character. The power conversion efficiency of over 7% has obtained by using thiophene unit.[47-52] Selenophene is the chalcogen homologue of thiophene with similar chemical and physical properties. However, selenophene has some advantages over thiophene in organic electronic applications.[53-55] The increase in conductivity can be obtained by the replacement of the sulfur atom by the selenium atom as a result of the stronger heteroatomic interaction enabling enhanced chain interaction and carrier transport ability.[56] In addition, selenophene containing polymers have more quinoidal character than thiophene counterparts which provides the π-conjugated connection to other moieties with lengthened π-conjugation along the polymer chain.[57,58] However, solubility of thiophene is higher than selenophene because of the more rigid structure of selenophene. As the size of heteroatom increases, the solubility and optical band gap decreases due to the stabilization of the LUMO level of polymer.[59] Structures of thiophene and selenophene are demonstrated in Figure 8.

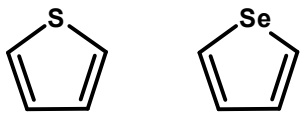

Figure 8. Structures of Thiophene and Selenophene

1.8.3. Benzo[1,2-b:4,5-b′]dithiophene Moiety

In donor-acceptor semiconducting copolymers, benzo[1,2-b:4,5-b′]dithiophene (BDT) is used as an electron donating unit due to its symmetric and planar conjugated structure that improve the π-π stacking of the polymer and thus increase the charge carrier mobility. In order to optimize the solubility and energy levels of polymers, several types of substituents can be covalently connected on BDT.[60-63] Structure of benzodithiophene is shown in Figure 9.

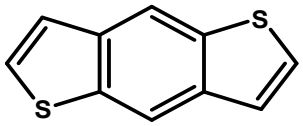

Figure 9. Structure of Benzo[1,2-b:4,5- b′]dithiophene

1.9. Applications of Conducting Polymers

In development of transmissive and reflective electrochromic devices, π-conjugated electrochromic polymers[64] are preferred due to their fine-tuning color,[65] fast switching capabilities,[66] high coloration efficiencies,[67,68] and high optical contrast ratios.[69] π-conjugated electrochromic devices are used as candidate materials in application areas such as electrochromic mirrors,[70] smart windows,[71] electronic paper,[72] etc. Additionally, π-conjugated polymers are favored in many device applications containing light-emitting diodes,[73] field-effect transistors,[74] memory devices[75] and photovoltaic cells.[76]

1.10. Electrochromism

A reversible optical change in a material induced by an external voltage is called electrochromism.[27] Conjugated polymers are one class of electrochromic (EC) materials, widely used due to their rapid response times, high optical contrasts, ease of processability and modification of their structure to create multicolor electrochromes. Derivatives of poly(thiophene), poly(aniline) and poly(pyrrole) are commonly used conjugated EC polymers.[28]

Electrochromic materials can be divided into three types according to their electronically accessible optical states. The first one consists of materials with at least one colored and one bleached state. Metal oxides, viologens and polymers like poly(3,4-ethylenedioxythiophene) (PEDOT) are some examples of these materials, specifically used for absorption/transmission-type device applications such as optical shutters and smart windows. Electrochromes with two distinctive colored states are the second type of EC materials. Although these materials do not have transmissive

state, they can be used for display-type applications where different colors are required in different redox states. For example, thin films of polythiophene switch from red to blue by oxidation. Depending on the redox state of the material, more than two color states are accessible in the third class of EC materials. Conjugated polymers are the most attractive examples due to their versatility for making laminates, blends and copolymers. In addition, polymers such as poly(aniline) and poly(3,4-propylenedioxypyrrole) are intrinsically multicolor EC polymers.[29]

1.10.1. Parameters in Identifying and Characterizing the Electrochromic Materials

1.10.1.1. Electrochromic Contrast

Electrochromic contrast (EC) is the percent transmittance change ($\Delta\%T$) at a specified wavelength where the optical contrast of the EC material is the highest. Measuring the relative luminance change gives overall electrochromic contrast.[30]

1.10.1.2. Coloration Efficiency

Coloration efficiency is used to determine the amount of charge necessary to produce the optical change. The power requirements of an EC material can be measured by coloration efficiency, also called as EC efficiency.

$$\eta = \frac{(\Delta OD)}{Q_d} = \frac{\log\left[\frac{T_b}{T_c}\right]}{Q_d}$$

η (cm^2/C) is the coloration efficiency at a given λ, (ΔOD) is the amount of optical density change, Q_d is the injected/ejected electronic charge and, T_b and T_c are the bleached and colored transmittance values, respectively.

1.10.1.3. Switching Speed

The time required for the coloring or bleaching process of an EC material is called as switching speed. It plays an important role in applications of dynamic displays and switchable mirrors. Ionic conductivity of the electrolyte, accessibility of the ions to the electroactive sites, film thickness, morphology of the thin film and magnitude of applied potential are the factors affecting the switching speed of EC materials.

1.10.1.4. Stability

Electrochromic stability is related with electrochemical stability because the loss of electrochromic contrast and the performance of EC material are caused by the degradation of the active redox couple. Irreversible oxidation or reduction at extreme potentials, *iR* loss of the electrolyte or electrode, heat release due to the resistive parts in the system and side reactions due to oxygen or water in the cell are responsible for common degradation.

1.10.1.5. Optical Memory

After the electric field is removed, the time the material sustains its absorption state is called as optical memory (open-circuit memory). While the optical memory is long in solid-state EC devices, the colored state bleaches rapidly in solution-based EC systems.[29]

1.11. Organic Solar Cells

Organic solar cell is a type of photovoltaic that converts sunlight into electricity by the photovoltaic effect. The most basic types of devices are single layer, bilayer heterojunction, bulk heterojunction and diffuse bilayer heterojunction. The main differences between the architectures of devices are the exciton dissociation or charge separation process, and successive charge transport to the electrodes.

1.11.1. Bulk Heterojunction Organic Solar Cells

In bulk heterojunction device, donor and acceptor components are mixed in a bulk volume in a way that each donor-acceptor interface exists in a shorter distance than the exciton diffusion length of each absorbing site. Charge separation occurs in interfacial area which is dispersed throughout bulk heterojunction device. Therefore, excitons are dissociated within their lifetime. As a result, there should be no loss theoretically. In addition, recombination of charges is decreased to a large extent due to charge separation within the different phases. In bulk heterojunction devices, percolated pathways for the hole and electron transporting phases to the contacts are required although acceptor and donor phases are selective in contacting cathode and anode. Generally, ITO is anode, PEDOT:PSS is hole transport layer, polymer:PCBM is active layer and Al is cathode parts of bulk heterojunction organic photovoltaic cell.[77] Bulk heterojunction device structure is shown in Figure 10.

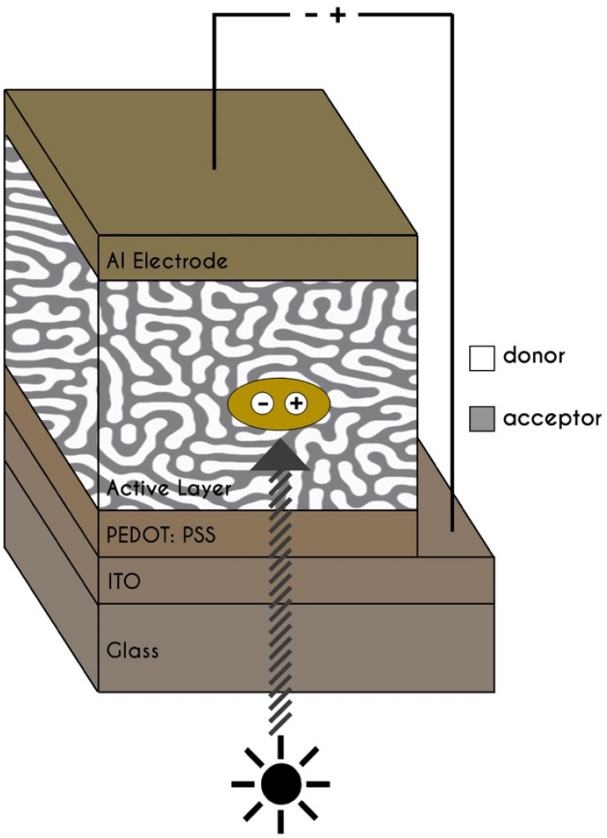

Figure 10. Bulk Heterojunction Device Structure

1.11.2. Working Principle of Organic Solar Cells

Conversion of light into electricity by an organic solar cell occurs via four main steps. First, light's energy is absorbed by polymer to create excitons, electron-hole pairs. Then, bound excitons travel to charge separation area and they separate into charges at the heterojunction, sending current to the contacts. Finally, electrons travel through active layer toward the metal cathode as electrical current while holes travel to anode.[78]

The electrical current obtained from a photovoltaic solar cell depends on the number of created charges, collected at the electrodes. Overall photocurrent efficiency (η_j) can be determined from the following equation.

$$\eta_j = \eta_{abs} \times \eta_{diss} \times \eta_{out}$$

η_{abs} is the fraction of photons absorbed, η_{diss} is the fraction of dissociated electron-hole pairs and η_{out} is the fraction of separated charges that reach the electrodes.[79]

1.11.3. Characterization of a Solar Cell Device

The current-voltage characteristics (I-V curve) of a solar cell in the dark and under illumination are demonstrated in Figure 11. There is almost no current flowing in the dark, until the contacts start to inject at forward bias for voltages higher than the open circuit voltage. The device generates power under light. The product between current and voltage and power output is the largest at maximum power point (MPP). MPP should be compared with incident light intensity in order to determine the efficiency of a solar cell. The power conversion efficiency (PCE) of solar cell is determined by the following equation.

$$PCE = \frac{V_{OC} \times I_{SC} \times FF}{P_{in}}$$

where V_{OC} is the open circuit voltage, I_{SC} is the short circuit current, FF is the fill factor and P_{in} is the incident light power density. The intensity of light is standardized at 1000 W/m^2.[77]

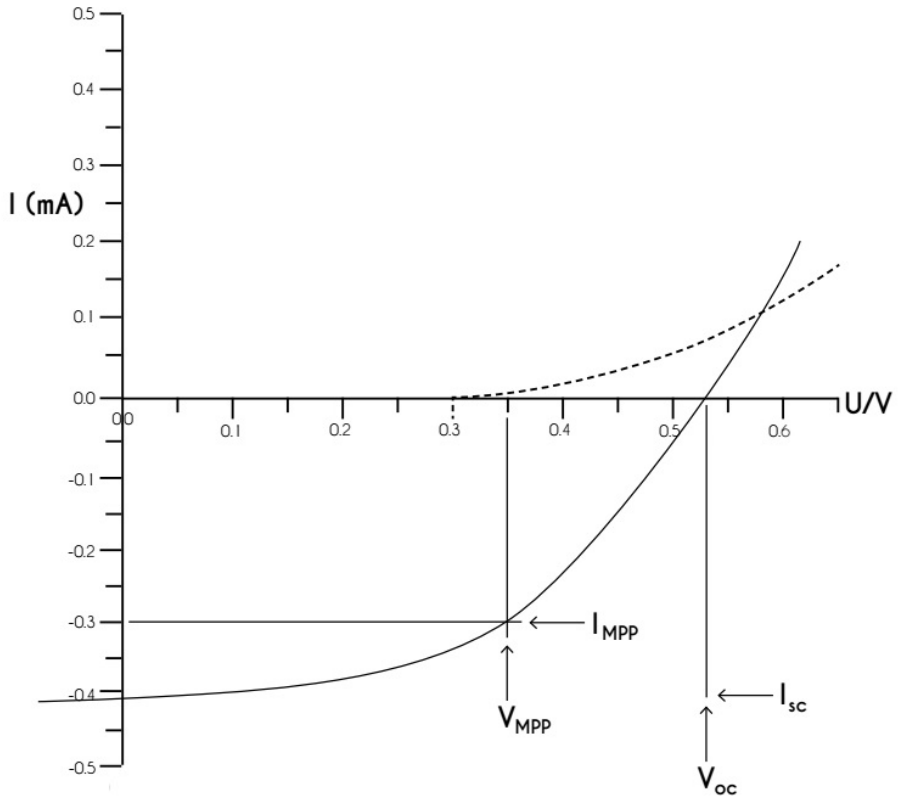

Figure 11. Current-Voltage curves of an organic solar cell (dark, ---; illuminated, —)

1.11.4. Critical Parameters Affecting Solar Cell Efficiency

1.11.4.1. Open Circuit Voltage

The maximum voltage a solar cell can provide to an external circuit is defined as open circuit voltage (V_{OC}). It can be obtained from the splitting hole and electron quasi-Fermi levels.[80] The maximum available voltage in a p-n junction is detected by the difference of the energy levels of n-doped and p-doped semiconductors which are the quasi Fermi levels of the two charge carriers. HOMO level of donor and LUMO

level of acceptor determine quasi Fermi levels of p-type and n-type semiconductors, respectively. The open circuit voltage is linearly dependent on HOMO level of donor and LUMO level of acceptor in organic solar cells.[81,82] Nanomorphology of the active layer affects V_{OC} in the polymer fullerene bulk heterojunction cells.[83] In organic light emitting diodes (OLEDs), open circuit voltage can be increased by cathode modification with LiF deposition between the metal electrode and organic semiconductor due to improved charge injection.[84-86]

$$V_{OC} = (1/q) (| E_{HOMO, Donor} | - | E_{LUMO, Acceptor} | - 0.3 \text{ V})$$

where q is the elementary charge and 0.3 V loss is an empirical value which may be greater or smaller in different systems. The reason of loss may be due to the tail states induced by the disorder in blend or the energy loss induced by recombination of carriers.

1.11.4.2. Short Circuit Current

The current through the solar cell when the voltage is zero is called short-circuit current (I_{SC}). It is the maximum current drawn from a solar cell. Generation and collection of light-generated carriers determine the I_{CS}. The short-circuit current density (J_{SC} in mA/cm^2) is more commonly used rather than I_{SC} in order to ignore the dependence of solar cell area.[77] The short circuit current density (J_{SC}) is a parameter to characterize the power conversion efficiency of a photovoltaic device. The information for current-loss analysis and device optimization can be obtained from a map of local J_{SC} of a solar cell at standard irradiance spectra.[87]

1.11.4.3. Fill Factor

For an organic solar cell, the fill factor (FF) is a substantial factor in determining the power conversion efficiency.[88]

$$FF = \frac{V_{MPP} \times I_{MP}}{V_{OC} \times I_{SC}}$$

When the built-in field is lowered toward the open circuit voltage, the fraction of photogenerated charge carriers reaching the electrodes becomes an important parameter in determining the FF. There is a rivalry between transport and recombination of charge carrier. Therefore, the distance (d) that charge carriers drifting under a certain electrical field (E) can be obtained from the following equation;

$$d = \mu \times \tau \times E$$

where lifetime and mobility are denoted as τ and μ, respectively.[89]
The product of $\mu \times \tau$ should be maximized in order to obtain large FF.[90] On the other hand, the series resistances should be minimized because finite conductivity of ITO substrate restricts the fill factor on solar cells having large area. In addition, in order to maximize the parallel shunt resistance, the device should be free of shorts between electrodes.[91]

1.12. Benzotriazole and Benzodithiophene Containing Polymer Solar Cells

In efficient organic solar cell applications, benzo[d][1,2,3]triazole (BTz) is used as an acceptor unit due to its electron poor nature and low-lying LUMO energy level. An appropriate donor unit should be selected in order to obtain wide absorption spectra and low band gap. Hence, selenophene substitution as π-bridge results in high mobility, enhanced light absorption and conductivity due to intermolecular Se-Se interactions. In addition, LUMO is lowered while HOMO of polymer is not

affected in selenophene-based polymers. As an additional donor unit, benzo[1,2-b:4,5-b′]dithiophene (BDT) can be used due to its planar conjugated structure ensuring high hole mobility and strong intramolecular charge transfer. In 2014, Unay et al. reported that the organic solar cell device based on polymer namely, **P-SBTBDT** consisting BTz and Se coupled with BDT as shown in Figure 12. The device showed the PCE of 3.60 % with **P-SBTBDT**:$PC_{71}BM$ (1:1, w/w).[92]

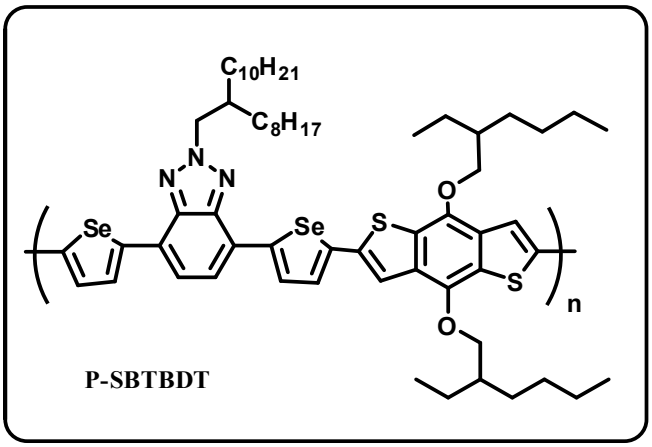

Figure 12. Structure of **P-SBTBDT**

In the article published in 2015 by Lee et al. it is reported that the performances of solar cell devices were affected by oligothienyl units introduced into the side chains by changing the molecular arrangement and packing, microstructure and crystalline behavior of polymer:$PC_{71}BM$ blend films. By tuning the π-conjugation length of side chains, the crystallinity and blend morphology of the polymers could be systematically controlled. π-conjugated side chains of alkyl-thienyl groups increased electron density and interchain aggregation among conjugating polymers, hence light absorption and charge transport properties were enhanced. Moreover, polymers with 2-alkylthienyl groups showed high hole mobility and broad absorption bands with the highest PCE of 6.48 % with **PBDT2FBT-T3**:$PC_{71}BM$ (1:0.8 w/w).[93] The abbreviated structure of **PBDT2FBT-Tm** is demonstrated in Figure 13, where m is 1, 2, 3 and 4.

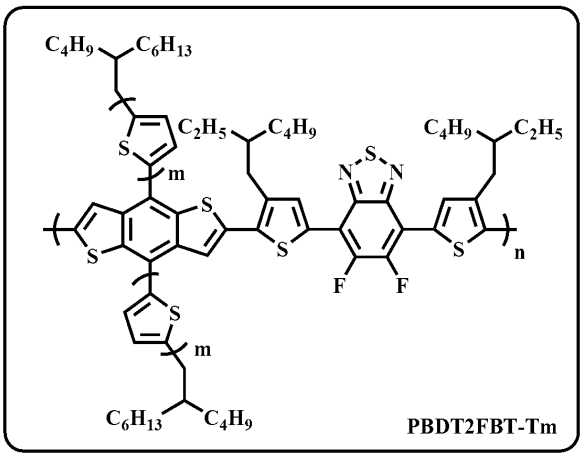

Figure 13. Structure of **PBDT2FBT-Tm** (m=1,2,3,4)

In 2014, Zhang et. al. reported that dihedral angles between the benzodithiophene and conjugated side groups had influence on the absorption bands, crystallinities, HOMO levels and aggregation sizes of the polymers. In addition, this study suggested that introducing conjugated side groups into BDT-based polymers with different steric hindrance could adjust both molecular energy levels and morphologies. The photovoltaic results indicated that **PBDTTT-EFT**:$PC_{71}BM$ (1:1.5 w/w) with 3% 1,8-diiodooctane (DIO) (v/v) as additive showed PCE of 9.0 % due to strong interchain π-π stacking effect of the polymer.[94] The structure of **PBDTTT-EFT** is illustrated in Figure14.

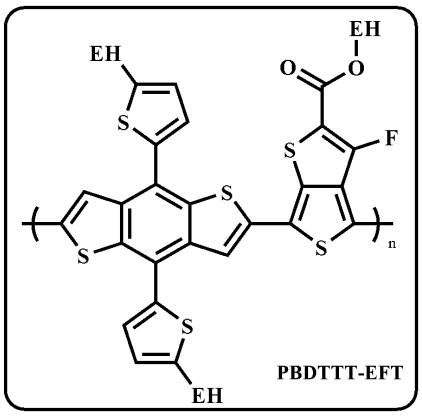

Figure 14. Structure of **PBDTTT-EFT**

In a study published 2015, Yin et. al. synthesized benzodithiophene based molecules with mono-thiophene as the π-conjugation bridge. The **DCV-1T-TBDT**:$PC_{61}BM$ (1:0.6, w/w) exhibited the highest power conversion efficiency of 4.48 %. In addition, it showed minor thickness-dependent PCE behavior in photovoltaic devices. The low thickness sensitivity of molecule demonstrated the feasibility for roll-to-roll fabrication.[95] The structure of **DCV-1T-TBDT** is shown in Figure 15.

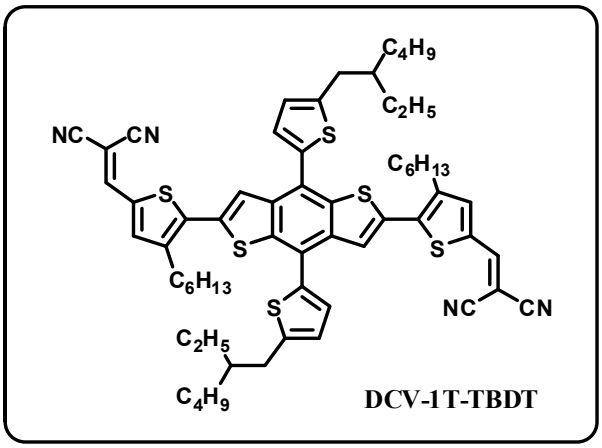

Figure 15. Structure of **DCV-1T-TBDT**

1.13. Aim of the Study

In order to synthesize low band gap polymers with high power conversion efficiency for organic solar cell applications, donor-acceptor approach was used. For that purpose, benzotriazole and benzodithiophene were used as acceptor and donor units, respectively. In addition, thiophene and selenophene were selected as π-bridge donor groups in designed polymers. Two novel polymers namely, **P-SBTBDTT** and **P-TBTBDTT** were synthesized via Stille coupling for solar cell applications. Structures of synthesized polymers are shown in Figure 16.

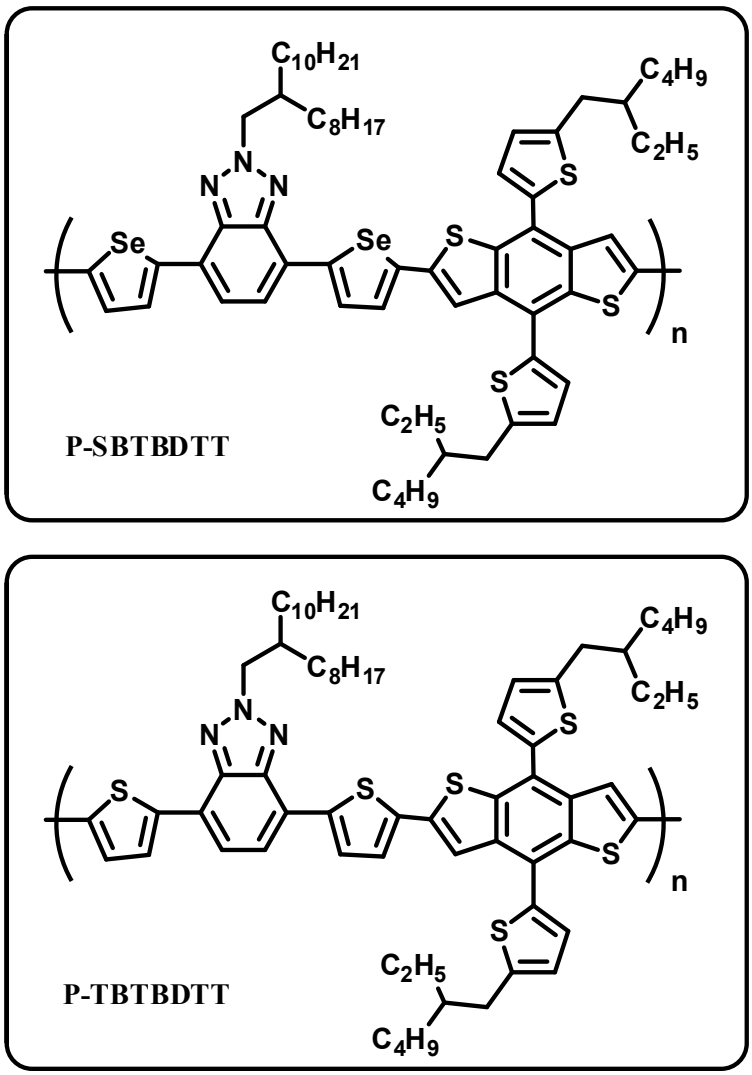

Figure 16. Synthesized Polymers

CHAPTER 2

EXPERIMENTAL

2.1 Materials and Equipments

All chemicals used in the synthesis were purchased from Sigma-Aldrich Chemical Co. Ltd. and TCI. Tetrahydrofuran (THF) was dried over sodium/benzophenone ketyl. Moisture and air sensitive reactions were conducted under argon atmosphere. Merck Silica Gel 60 was used for the purification of synthesized materials as the stationary phase in column chromatography. Bruker Spectrospin Avance DPX-400 Spectrometer with trimethylsilane (TMS) as the internal reference was used to record ^{1}H and ^{13}C spectra of chemical structures. The chemical shifts determined relative to $CDCl_3$, giving peaks at 7.26 and 77 ppm for the ^{1}H and ^{13}C NMR, respectively. UV-Vis spectra analyses were performed by Varian Cary 5000 UV-Vis spectrophotometer at room temperature. Polymer Laboratories GPC 220 with polystyrene as the standard and chloroform as the solvent was used in order to calculate average molecular weight of the polymer. Organic solar cells were fabricated in a MBRAUN glove-box system under inert atmosphere. Current density-voltage characteristics were observed using Keithley 2400 under illumination of Atlas Material Testing Solutions solar simulator (AM 1.5 G).

2.2. Synthesis of Monomers

Synthetic pathway of synthesized monomers was demonstrated in Figure 17. 4,7-dibromo-2-(2-octyldodecyl)-2H-benzo[d][1,2,3]triazole **(1)**, tributyl(thiophen-2-yl)stannane **(2)** and tributyl(selenophen-2-yl)stannane **(3)** were synthesized according to previously published procedures.[42, 96-99] Compound **1** was separately coupled with compound **2** and **3** via Stille coupling reactions. Then, bromination of compounds were performed in the presence of NBS in order to obtain desired monomers according previously reported methods.[100]

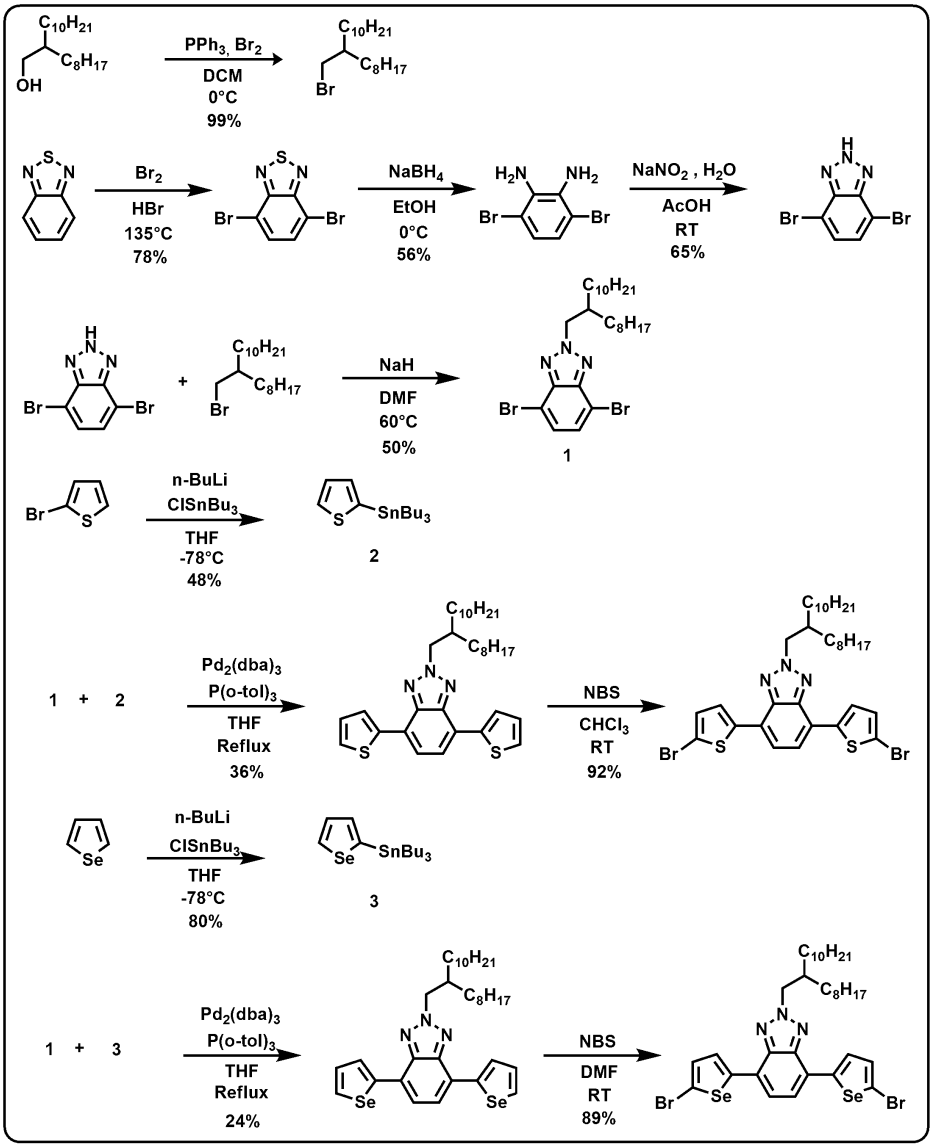

Figure 17. Synthetic pathway of synthesized monomers

2.2.1. Synthesis of 9-(bromomethyl)nonadecane

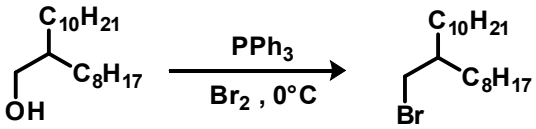

Figure 18. Synthesis of 9-(bromomethyl)nonadecane

2-Octyl-1-dodecanol (5.0 g, 17 mmol) was dissolved in 50 mL dichloromethane (DCM). Then, PPh_3 (4.6 g, 17.6 mmol) was added to the solution at 0°C. 1 mL bromine was then added and the reaction was stirred for 30 minutes. Then, the mixture was warmed to room temperature and washed with $NaHSO_3$ and distilled water. The organic layer was dried over Na_2SO_4 and the solvent was evaporated under reduced pressure. The residue was purified by column chromatography (hexane, silica gel) to obtain 9-(bromomethyl)nonadecane (5.98 g, yield 99%) as a colorless oil.

^{1}H NMR (400 MHz, $CDCl_3$), δ (ppm): 3.44 (d, J = 4.7 Hz, 2H), 1.59 (m, 1H), 1.27 (m, 32H), 0.89 (t, J = 6.7 Hz, 6H). ^{13}C NMR (100 MHz, $CDCl_3$), δ (ppm): 39.6, 39.5, 32.59, 31.9, 29.8, 29.7, 29.6, 29.5, 29.4, 29.3, 26.6, 22.7, 14.1.

2.2.2. Synthesis of 4,7-dibromobenzo[c][1,2,5]thiadiazole

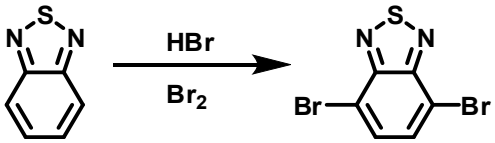

Figure 19. Synthesis of 4,7-dibromobenzo[c][1,2,5]thiadiazole

Benzo-1,2,5-thiadizole (10.0 g, 73.4 mmol) was dissolved in 75 mL HBr (47%) at room temperature. Then, a solution of Br_2 (35.2 g, 220 mmol) in HBr (15 mL) was added to the reaction mixture slowly. After addition was completed, the reaction mixture was refluxed overnight at 135°C. Then, the reaction was filtered after

cooling the mixture to room temperature to obtain an orange solid residue. $NaHSO_3$(aq) was used in washing process of residue in order to consume excess Br_2. Later, the residue was washed with cold diethyl ether several times to obtain 4,7-dibromobenzo[c][1,2,5]thiadiazole (16.9 g, yield 78%) as a yellow solid.

2.2.3. Synthesis of 3,6-dibromobenzene-1,2-diamine

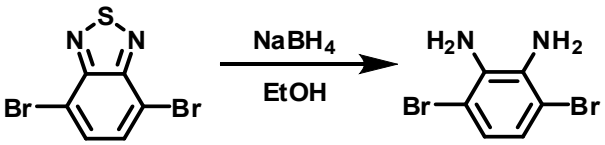

Figure 20. Synthesis of 3,6-dibromobenzene-1,2-diamine

In 1 L round bottom flask, 4,7-dibromobenzothiadiazole (10.0 g, 34.0 mmol) was dissolved in 100 mL ethanol (EtOH). In an ice bath, the mixture was cooled to 0°C. Then $NaBH_4$ powder (32 g, 0.85 mol) was added portionwise to reaction mixture. The reaction was warmed to room temperature when gas evolution stopped. Then the reaction was stirred for 20 hours. After evaporation of the solvent, the mixture was extracted with Et_2O and the organic phase was washed with brine. Afterward, the organic phase was separated and the solvent was evaporated under reduced pressure to obtain 3,6-dibromobenzene-1,2-diamine (5.1 g, yield 56%) as a faint yellow solid.

2.2.4. Synthesis of 4,7-dibromo-2H-benzo[d][1,2,3]triazole

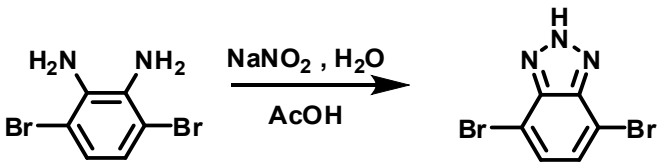

Figure 21. Synthesis of 4,7-dibromo-2H-benzo[d][1,2,3]triazole

A solution of $NaNO_2$ (1.88 g, 20.7 mmol) in H_2O (36 mL) was slowly added to 3,6-dibromobenzene-1,2-diamine (5.0 g, 19 mmol) solution in 75 mL acetic acid (AcOH). The mixture was stirred at room temperature for 20 minutes. After filtration, the precipitate was washed with distilled water several times to obtain 4,7-dibromo-2H-benzo[d][1,2,3]triazole (3.74 g, yield 65%) as a pink powder.

2.2.5. Synthesis of 4,7-dibromo-2-(2-octyldodecyl)-2H-benzo[d][1,2,3]triazole

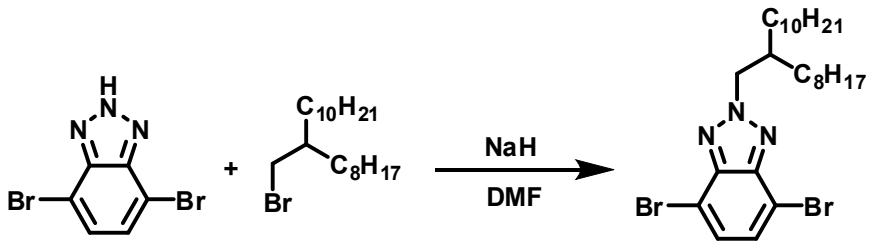

Figure 22. Synthesis of 4,7-dibromo-2-(2-octyldodecyl)-2H-benzo[d][1,2,3]triazole

Under argon atmosphere, 4,7-dibromo-2H-benzo[d][1,2,3]triazole (1.78 g, 6. 4 mmol) was dissolved in 15 mL dimethylformamide (DMF). Then, NaH (181 mg, 7.5 mmol) was added to reaction mixture at 0°C. After addition of 9-(bromomethyl)nonadecane (2.72 g, 7.5 mmol) at 60°C, the reaction was stirred at 70°C overnight. The mixture was extracted with Et_2O and the organic phase was washed with distilled water. Organic layer was separated and dried over Na_2SO_4. Then, solvent was evaporated under reduced pressure. Column chromatography was performed by using silica gel and 4,7-dibromo-2-(2-octyldodecyl)-2H-benzo[d][1,2,3]triazole was obtained as faint yellow oil (1.79 g, yield 50%).

^{1}H NMR (400 MHz, $CDCl_3$), δ (ppm): 7.29 (s, 2H), 4.62 (d, J = 7.2 Hz, 2H), 2.27 (m, 1H), 1.15 (m, 32H), 0.80 (m, 6H). ^{13}C NMR (100 MHz, $CDCl_3$), δ (ppm): 143.56, 129.30, 109.97, 60.99, 38.97, 34.63, 31.91, 31.85, 31.58, 31.15, 29.76, 29.60, 29.59, 29.46, 29.41, 29.34, 29.24, 26.88, 26.01, 25.24, 22.68, 22.65, 14.10.

2.2.6. Synthesis of Tributyl(selenophen-2-yl)stannane

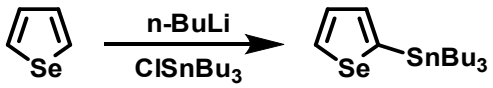

Figure 23. Synthesis of Tributyl(selenophen-2-yl)stannane

Selenophene (2.25 g, 17.2 mmol) was dissolved in 25 mL dry tetrahydrofuran (THF). Then, the reaction was cooled to -78°C under argon atmosphere and 7.7 mL 2.7 M n-BuLi in hexane was added dropwise to reaction mixture. The reaction mixture was stirred for 1 hour after addition of n-BuLi was completed. Then, stannyltributyltinchloride (5.1 mL, 19 mmol) was slowly added to the reaction mixture. The reaction mixture was stirred for 1.5 hours at -78°C after addition was completed. Then, it was warmed to room temperature and stirred overnight. Solvent was evaporated under reduced pressure and the mixture was extracted with Et_2O and the organic phase was washed with water. Then, organic phase was separated and dried over Na_2SO_4. The residue was purified by using neutral alumina column chromatography with hexane eluent and tributyl(selenophen-2-yl)stannane (5.8 g, yield 80%) was obtained as colorless oil.

^{1}H NMR (400 MHz, $CDCl_3$), δ (ppm): 8.39 – 8.11 (m, 1H), 7.40 (m, 2H), 1.49 (m, 7H), 1.27 (m, 8H), 1.03 (m, 6H) 0.82 (t, 12H).

2.2.7. Synthesis of 2-(2-octyldodecyl)-4,7-di(selenophen-2-yl)-2H-benzo[d][1,2,3]triazole

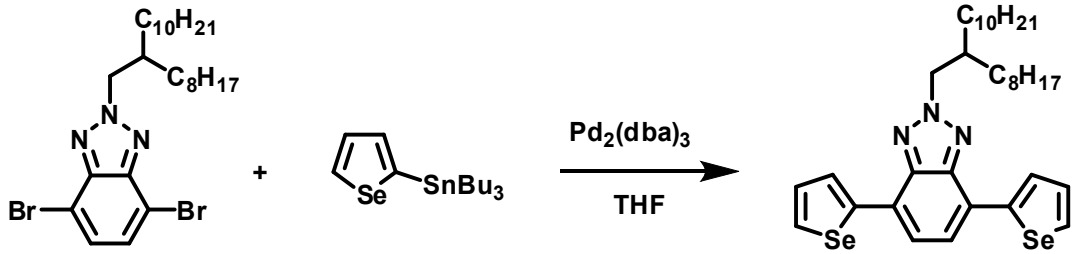

Figure 24. Synthesis of 2-(2-octyldodecyl)-4,7-di(selenophen-2-yl)-2H-benzo[d][1,2,3]triazole

4,7-dibromo-2-(2-octyldodecyl)-2H-benzo[d][1,2,3]triazole (850 mg, 1.52 mmol) and tributyl(selenophen-2-yl)stannane (1.7 g, 4.0 mmol) were dissolved in dry THF (25 mL). $Pd_2(dba)_3$ (69.81 mg, 0.076 mmol) and o-tolyl-phosphine (186 mg, 0.61 mmol) was added into the solution. Then, the reaction mixture was refluxed for 18 hours under argon atmosphere. Solvent was removed under reduced pressure after the reaction was completed. The residue was purified by column chromatography by using silica gel and 2-(2-octyldodecyl)-4,7-di(selenophen-2-yl)-2H-benzo[d][1,2,3]triazole (240 mg, yield 24%) was obtained as a yellow solid.

^{1}H NMR (400 MHz, $CDCl_3$), δ (ppm): 8.19 (dd, J = 3.9, 0.9 Hz, 2H), 8.08 (dd, J = 5.6, 0.9 Hz, 2H), 7.61 (s, 2H), 7.42 (dd, J = 5.6, 3.9 Hz, 2H), 4.75 (d, J = 6.4 Hz, 2H), 2.42 – 2.16 (m, 1H), 1.55 (m, 7H), 1.25 (m, 24H), 0.87 (td, J = 6.7, 3.9 Hz, 6H).

^{13}C NMR (100 MHz, $CDCl_3$), δ (ppm): 143.7, 140.3, 130.0, 128.9, 126.6, 123.9, 121.3, 75.6, 75.3, 37.7, 30.5, 30.4, 30.1, 28.4, 28.2, 28.1, 27.9, 24.9, 21.3, 12.7.

2.2.8. Synthesis of 4,7-bis(5-bromoselenophen-2-yl)-2-(2-octyldodecyl)-2H-benzo[d][1,2,3]triazole

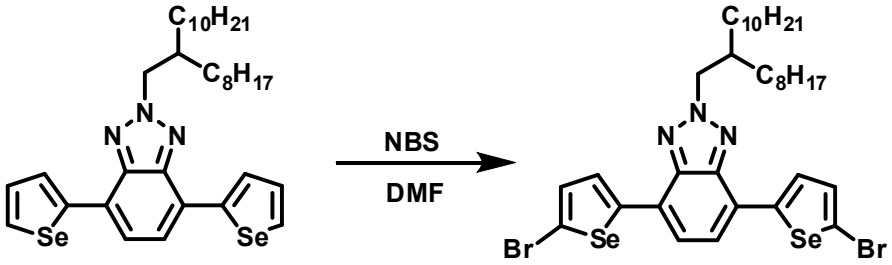

Figure 25. Synthesis of 4,7-bis(5-bromoselenophen-2-yl)-2-(2-octyldodecyl)-2H-benzo[d][1,2,3]triazole

2-(2-octyldodecyl)-4,7-di(selenophen-2-yl)-2H-benzo[d][1,2,3]triazole (190 mg, 0.29 mmol) was dissolved in anhydrous DMF (10 mL). Then, N-bromosuccinimide (NBS) (120 mg, 0.72 mmol) was added. Under argon atmosphere, the mixture was stirred at room temperature for 18 hours. The solvent was removed under reduced pressure and the mixture was extracted with Et_2O and the organic phase was washed with water. Column chromatography was performed by using silica gel and 4,7-bis(5-bromoselenophen-2-yl)-2-(2-octyldodecyl)-2H-benzo[d][1,2,3]triazole (210 mg, yield 89%) was obtained as dark yellow solid.

^{1}H NMR (400 MHz, $CDCl_3$), δ (ppm): 7.78 (d, J = 4.2 Hz, 2H), 7.54 (s, 2H), 7.33 (d, J = 4.2 Hz, 2H), 4.73 (d, J = 6.4 Hz, 2H), 2.40 – 2.19 (m, 1H), 1.25 (m, 32H), 0.88 (m, 6H). ^{13}C NMR (100 MHz, $CDCl_3$), δ (ppm): 132.6, 126.3, 133.5, 132.6, 130.7, 129.0, 126.1, 114.8, 77.3, 77.0, 76.7, 31.9, 31.5, 29.9, 29.6, 29.3, 26.3, 22.7, 14.1.

2.2.9. Synthesis of Tributyl(thiophen-2-yl)stannane

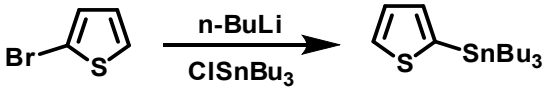

Figure 26. Synthesis of Tributyl(thiophen-2-yl)stannane

2-Bromothiophene (2.0 g, 12 mmol) was dissolved in dry THF (17 mL) at room temperature. Then, the reaction was cooled to -78°C under argon atmosphere and 2.7 M n-BuLi in toluene (5 mL) was dropwisely added to the reaction mixture. The reaction mixture was stirred for 1 hour after addition of n-BuLi was completed. Then, stannyltributyltinchloride (3.7 mL, 14 mmol) was slowly added to the reaction mixture. The reaction mixture was stirred for 1.5 hours at -78°C after addition was completed. Then, it was warmed to room temperature and stirred overnight. Solvent was evaporated under reduced pressure and extraction was performed with chloroform and brine. Then, organic phase was separated and dried over Na_2SO_4. Tributyl(thiophen-2-yl)stannane was obtained as pale yellow oil. (2.19 g, yield 48%) was obtained as colorless oil.

^{1}H NMR (400 MHz, $CDCl_3$), δ (ppm): 7.54 (d, 1H), 7.10 (d, 1H), 1.48 (t, 6H), 1.25 (dd, 6H), 0.81 (t, 9H).

2.2.10. Synthesis of 2-dodecyl-4,7-di(thiophen-2-yl)-2H-benzo[d][1,2,3]triazole

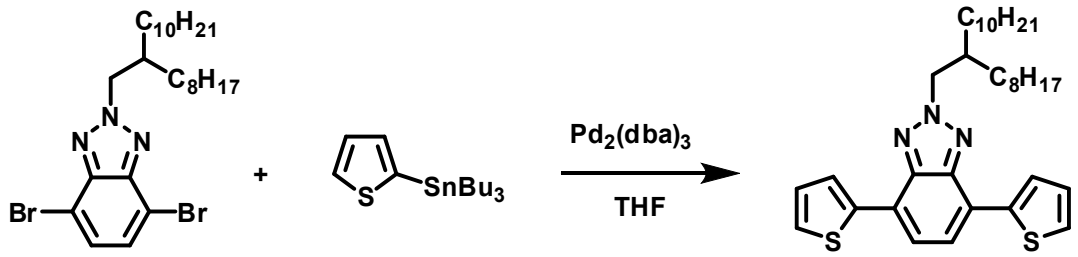

Figure 27. Synthesis of 2-dodecyl-4,7-di(thiophen-2-yl)-2H-benzo[d][1,2,3]triazole

4,7-dibromo-2-(2-octyldodecyl)-2H-benzo[d][1,2,3]triazole (1.0 g, 1.8 mmol) and tributyl(thiophen-2-yl)stannane (2.0 g, 5.4 mmol) were dissolved in 25 mL dry THF. $Pd_2(dba)_3$ (82 mg, 0.1 mmol) and o-tolyl-phosphine (218 mg, 0.7 mmol) was added into the solution. Then, the reaction mixture was refluxed for 18 hours under argon atmosphere. Solvent was removed under reduced pressure after the reaction was completed. The residue was purified by column chromatography by using silica gel and 2-dodecyl-4,7-di(thiophen-2-yl)-2H-benzo[d][1,2,3]triazole (360 mg, yield 36%) was obtained as a yellow solid.

^{1}H NMR (400 MHz, $CDCl_3$), δ (ppm): 8.10 (dd, J = 3.6, 1.1 Hz, 2H), 7.64 (s, 2H), 7.38 (dd, J = 5.1, 1.1 Hz, 2H), 7.18 (dd, J = 5.1, 1.1 Hz, 2H), 4.75 (d, J = 6.6 Hz, 2H), 2.33 (m, 1H), 1.39 (dd, 7H), 1.24 (d, 24H), 0.87 (dd, 6H).

2.2.11. Synthesis of 4,7-bis(5-bromothiophen-2-yl)-2-(2-octyldodecyl)-2H-benzo[d][1,2,3]triazole

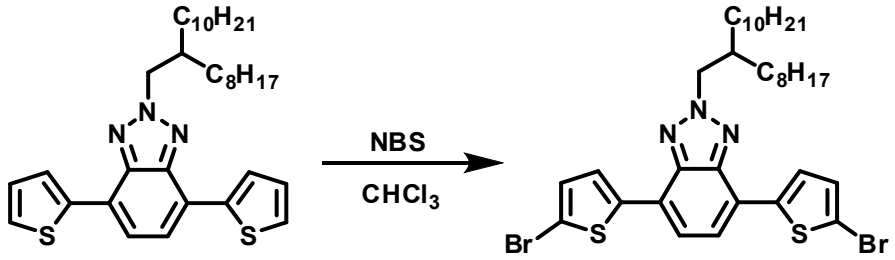

Figure 28. Synthesis of 4,7-bis(5-bromothiophen-2-yl)-2-(2-octyldodecyl)-2H-benzo[d][1,2,3]triazole

2-Dodecyl-4,7-di(thiophen-2-yl)-2H-benzo[d][1,2,3]triazole (180 mg, 0.3 mmol) was dissolved in 30 mL $CHCl_3$. Then, NBS (122 mg, 0.7 mmol) was added to the reaction mixture slowly under dark. Under argon atmosphere, the mixture was stirred at room temperature overnight. The solvent was removed under reduced pressure and extraction was carried out with chloroform and distilled water. Column chromatography was performed by using silica gel and 4,7-bis(5-bromothiophen-2-yl)-2-(2-octyldodecyl)-2H-benzo[d][1,2,3]triazole (180 mg, yield 92%) was obtained as green solid.

^{1}H NMR (400 MHz, $CDCl_3$), δ (ppm): 7.78 (d, J = 3.9 Hz, 2H), 7.54 (s, 2H), 7.12 (d, J = 3.9 Hz, 2H), 4.73 (d, J = 6.6 Hz, 2H), 2.29 (d, J = 5.9 Hz, 1H), 1.41-1.31 (m, 6H), 1.23 (d, J = 8.2 Hz, 26H), 0.86 (m, 6H). ^{13}C NMR (100 MHz, $CDCl_3$), δ (ppm): 141.59, 141.29, 130.88, 126.86, 122.97, 122.16, 113.14, 39.20, 31.94, 31.91, 31.46, 29.91, 29.68, 29.61, 29.37, 29.34, 26.27, 22.71, 14.15.

2.3. Synthesis of Polymers

Polymers namely **P-SBTBDTT** and **P-TBTBDTT** were synthesized via Stille coupling reactions in the presence of $Pd_2(dba)_3$ and o-tolyl-phosphine in THF solvent. Polymers were purified via Soxhlet extraction with methanol, acetone, hexane and chloroform.

2.3.1. Synthesis of P-SBTBDTT

4,7-Bis(5-bromoselenophen-2-yl)-2-(2-octyldodecyl)-2H-benzo[d][1,2,3]triazole (85.7 mg, 0.10 mmol) and 4,8-bis[5-(2-ethylhexyl)thiophene-2-yl]-2,6-bis(trimethylstannyl)benzo[1,2-b:4,5-b']dithiophene (100 mg, 0.11 mmol) were dissolved in 10 mL dry THF. $Pd_2(dba)_3$ (4.82 mg, 0.0053 mmol) and o-tolyl-phosphine (12.82 mg, 0.042 mmol) was added into the solution as catalyst and co-catalyst, respectively. After refluxing the reaction mixture for 23 hours under argon atmosphere, 2-bromothiophene (34.33 mg, 0.21 mmol) was added as end-capping reagent. 3 hours later, trimethyl(thiophen-2-yl)stannane (157.16 mg, 0.42 mmol) was added as the other end-capper. Solvent was removed under reduced pressure after the reaction was completed. The polymer was precipitated in cold methanol. Soxhlet extraction was performed for purification with acetone and hexane. Polymer was recovered by chloroform. After evaporation of solvent, **P-SBTBDTT** was obtained as purple solid. *GPC: Mn: 6500, Mw: 9300, PDI: 1.43.*

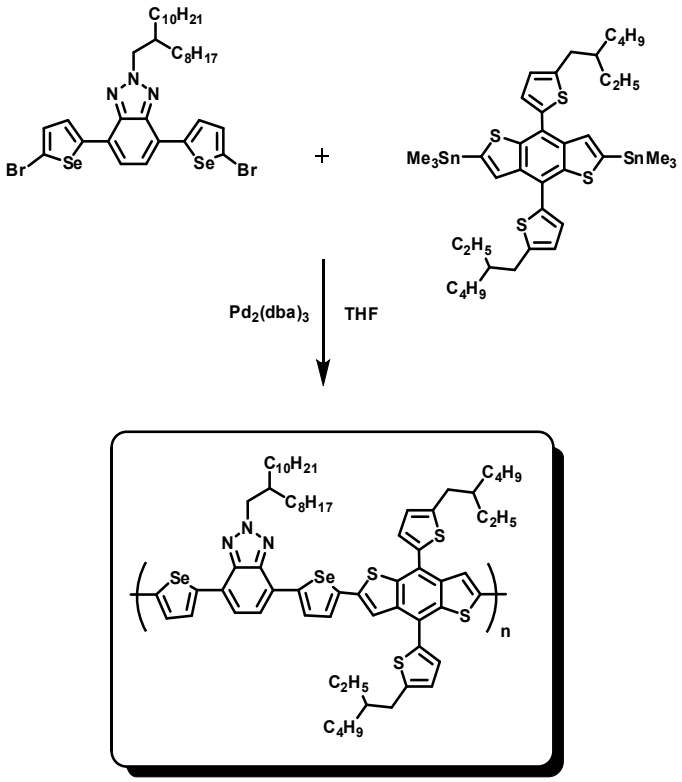

Figure 29. Synthesis of **P-SBTBDTT**

2.3.2. Synthesis of P-TBTBDTT

4,7-Bis(5-bromothiophen-2-yl)-2-(2-octyldodecyl)-2H-benzo[d][1,2,3]triazole (76 mg, 0.10 mmol) and 4,8-bis[5-(2-ethylhexyl)thiophene-2-yl]-2,6-bis(trimethylstannyl)benzo[1,2-b:4,5-b']dithiophene (100 mg, 0.11 mmol) were dissolved in 10 mL dry THF. $Pd_2(dba)_3$ (4.82 mg, 0.0053 mmol) and o-tolyl-phosphine (12.82 mg, 0.042 mmol) was added into the solution as catalyst and co-catalyst, respectively. Then, the reaction mixture was refluxed for 23 hours under argon atmosphere and 2-bromothiophene (34.33 mg, 0.21 mmol) was added as end-capper. The reaction was stirred for 3 hours and trimethyl(thiophen-2-yl)stannane (157.16 mg, 0.42 mmol) was added as the other end-capping reagent. Solvent was removed under reduced pressure after the reaction was completed. The polymer was precipitated in cold methanol. Soxhlet extraction was performed for purification with acetone and hexane. Polymer was recovered by chloroform. After evaporation of solvent, **P-TBTBDTT** was obtained as purple solid. *GPC: Mn: 9200, Mw: 12900, PDI: 1.40.*

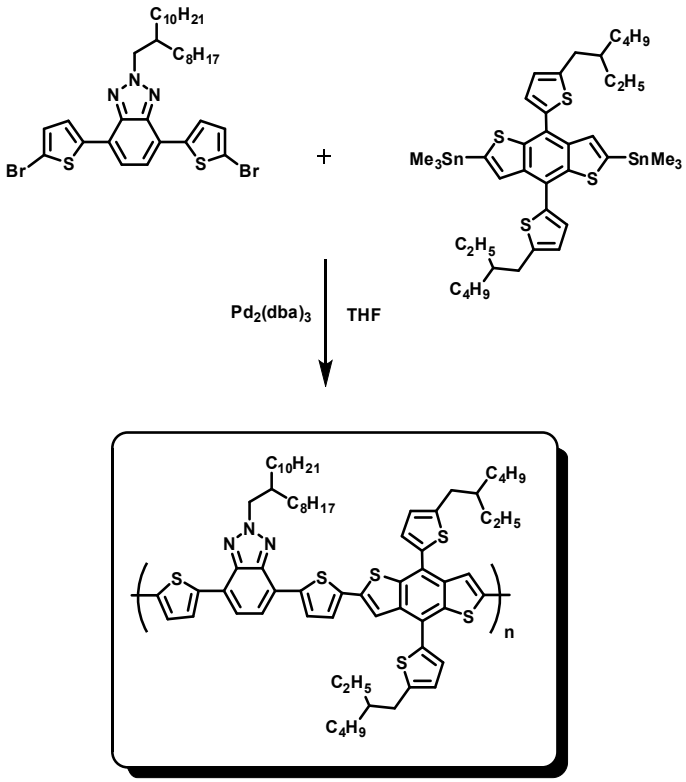

Figure 30. Synthesis of **P-TBTBDTT**

2.4. Characterization of Conducting Polymers

2.4.1. Gel Permeation Chromatography

Molecular weight and polydispersity index (PDI) of polymers were determined by gel permeation chromatography (GPC) technique. Polystyrene standards were used to calibrate the instrument. GPC consists of solid stationary phase and liquid mobile phase. The separating mechanism depends on the size of polymer molecules.

2.4.2. Electrochemical Studies

In order to investigate redox behaviors of polymers and calculate their HOMO and LUMO energy levels, cyclic voltammetry (CV) technique was performed. In this study, polymers were dissolved in chloroform. Then, indium tin oxide (ITO) surfaces were covered by spray coating. Potentiostat was used with three-electrode system. ITO, platinum and silver wire were used as working electrode (WE), counter electrode (CE) and reference electrode (RE), respectively. Polymer coated ITO was immersed into 0.1 M tetrabutylammonium hexafluorophosphate ($TBAPF_6$) in acetonitrile (ACN) solution in a quartz cuvette and redox reactions were monitored at a constant rate by using Gamry Instrument Reference 600 Potentiostat. In addition, color changes of polymers were observed. As a result, current density was plotted versus applied voltage.

2.4.3. Spectroelectrochemical Studies

Spectroelectrochemical studies were also performed by using three-electrode system in a quartz cell filled with $TBAPF_6$/ACN electrolyte solution. UV-Vis-NIR spectrum of polymers as a function of applied potential was used to determine neutral states of polymers besides polaron and bipolaron bands. These studies proved the color change in electrochemical studies and gave information about optical band gaps (E_g^{op}) and maximum absorption wavelengths (λ_{max}) of polymers.

2.4.4. Kinetic Studies

Chronoamperometric studies were carried out to determine optical contrast and switching time of polymers. Square wave potential was applied to polymer coated ITO glass slides in 0.1 M $TBAPF_6$/ACN solvent/electrolyte couple and transmittance change between oxidized and reduced states of polymers in Vis and NIR regions were monitored as a function of time. As a result, their optical contrasts were obtained and their switching times were calculated.

2.4.5. Photovoltaic Studies

The bulk heterojunction organic solar cell devices were fabricated with the structure of ITO/PEDOT:PSS/Polymer:$PC_{71}BM$/LiF/Al. First, ITO coated glass substrates were etched using HCl. Then, substrates were washed in ultrasonic bath for 15 minutes by using toluene, detergent, water and isopropyl alcohol. Substrates were dried by nitrogen gun and put into Harrick Plasma Cleaner. PEDOT:PSS was filtered through 0.45 μm PVDF syringe filter and coated onto ITO surface by spin coating. Later on, substrates were dried at 130°C for 20 minutes in order to evaporate water. Polymer:$PC_{71}BM$ mixtures were prepared with different ratios and filtered through 0.2 μm PTFE syringe filter. The mixtures were coated on PEDOT:PSS layer by G3P-8 spin coater in glove-box filled with nitrogen. Then, LiF and Al layers were evaporated through shadow mask and coated on polymer:$PC_{71}BM$ layer. Finally, current density-voltage characteristics were tested using Keithley 2400 under illumination of Atlas Material Testing Solutions solar simulator (AM 1.5 G).

CHAPTER 3

RESULTS AND DISCUSSION

3.1 Electrochemical Studies

Cyclic voltammetry analyses were carried out in order to investigate HOMO and LUMO energy levels of synthesized polymers, and their band gap energies. The corresponding values gave information about polymers whether they are suitable for optoelectronic applications or not. In order to perform these studies, polymers which were dissolved in chloroform were coated onto ITO surfaces via spray coating. Oxidation and reduction potentials of the polymers were observed by using three-electrode system. The system consisted of polymer coated ITO substrate, platinum and silver wire in quartz cell containing $TBAPF_6$/ACN electrolyte solution. Cyclic voltammograms were obtained at a scan rate of 100 mV/s. Analyses demonstrated that both of the polymers have p-doping and n-doping characters. While p-type doping/dedoping peaks of **P-SBTBDTT** were observed as 0.80 V/0.59 V, n-type doping/dedoping peaks were at -1.71 V/-1.35 V. On the other hand, **P-TBTBDTT** showed a reversible redox couple at 0.95 V/0.74 V and -1.89 V/-1.57 V as a consequence of p-type and n-type doping/dedoping processes, respectively. The cyclic voltammograms of these two polymers were demonstrated in Figure 31.

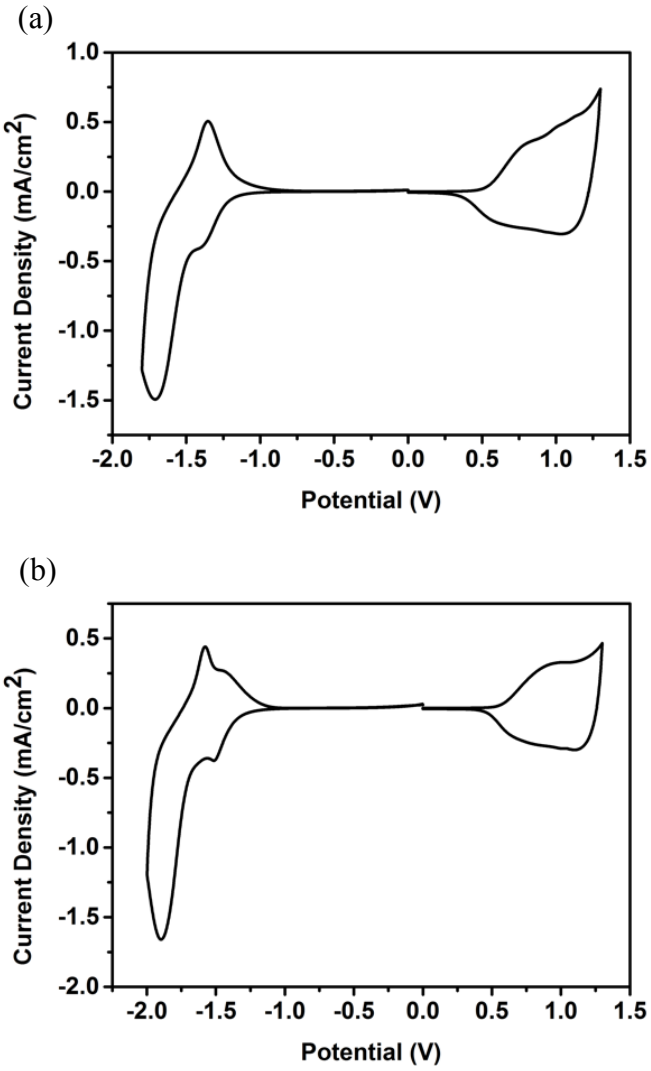

Figure 31. Single-scan cyclic voltammograms of polymer films in 0.1 M $TBAPF_6$ / ACN electrolyte solution (a) **P-SBTBDTT** (b) **P-TBTBDTT**

HOMO and LUMO energy levels of the polymers were calculated from the following equations by using CV data since they were both p- and n-dopable.

$$HOMO = -(4.75 + E_{ox,onset})$$

$$LUMO = -(4.75 + E_{red,onset})$$

The onset potentials of oxidation and reduction were determined from the tangent lines. As a result, HOMO energy levels of **P-SBTBDTT** and **P-TBTBDTT** were calculated as -5.27 eV and -5.30 eV whereas LUMO energy levels were -3.33 eV and -3.10 eV, respectively. In addition, electronic band gap (E_g^{el}) of the polymers were obtained from the following formula and E_g^{el} values were found as 1.96 eV and 2.2 eV for **P-SBTBDTT** and **P-TBTBDTT,** sequentially.

$$E_g^{el} = HOMO - LUMO$$

The results of electrochemical studies were summarized in Table 1.

Table 1. Summary of Electrochemical Properties

	P-SBTBDTT	**P-TBTBDTT**
$E_{p\text{-doping}}$ (V)	0.80	0.95
$E_{p\text{-dedoping}}$ (V)	0.59	0.74
$E_{n\text{-doping}}$ (V)	-1.71	-1.89
$E_{n\text{-dedoping}}$ (V)	-1.35	-1.57
HOMO (eV)	-5.28	-5.30
LUMO (eV)	-3.32	-3.10
E_g^{el} (eV)	1.96	2.2

Selenophene based polymer exhibited lower oxidation potential than the thiophene analogue due to its higher electron donating ability. More electron rich and more quinoidal character of selenophene than thiophene resulted in reduction of electronic band gap. Therefore, selenophene based **P-SBTBDTT** had 0.24 eV lower electronic band gap than thiophene based **P-TBTBDTT** that could lead increase in the amount of harvested photons in photovoltaic applications.

3.1.1. Scan Rate Studies

Anodic and cathodic current density values of polymers were determined in given potential at different scan rates. According to analyses, the mass transfer of anions in electrolyte solution to polymer surfaces were non-diffusion controlled due to linear relationship between current density and scan rate plots. In addition, both of the **P-SBTBDTT** and **P-TBTBDTT** demonstrated reversible redox processes considering cyclic voltammograms in Figure 32.

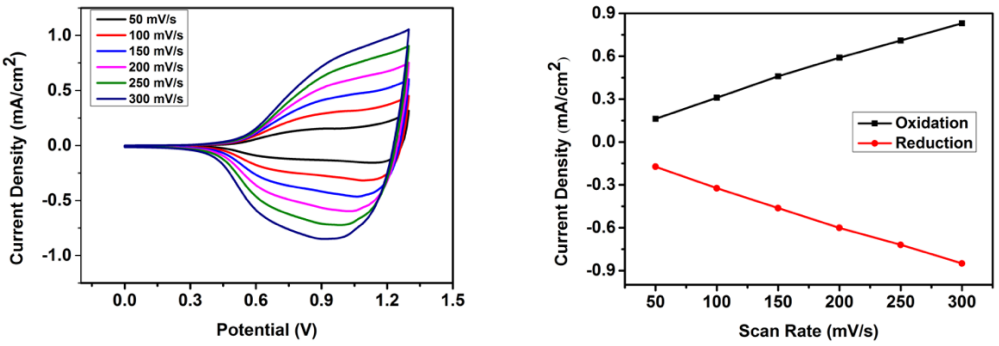

P-SBTBDTT

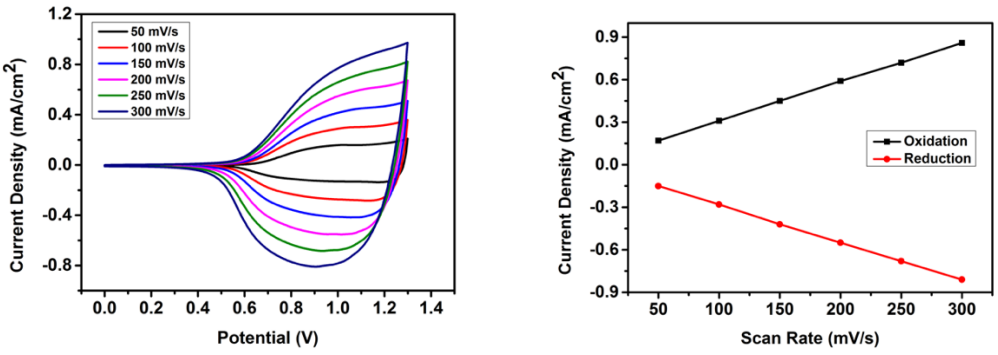

P-TBTBDTT

Figure 32. Scan rate studies of polymers in 0.1 M $TBAPF_6$ / ACN electrolyte solution

3.2 Spectroelectrochemical Studies

In spectroelectrochemical studies, light absorption behaviors of polymers in UV-Vis-NIR regions were analyzed as a function of wavelength as shown in Figure 33. Absorption peaks observed in the visible region indicated π-π* transition between HOMO and LUMO energy levels of polymers. **P-SBTBDTT** showed maximum absorption peaks (λ_{max}) at 540 nm/590 nm while **P-TBTBDTT** exhibited peaks at 519 nm/561 nm. Thus, **P-SBTBDTT** showed red shift absorption with 21 nm/29 nm compared to **P-TBTBDTT**. Higher electron donating ability and more quinoidal character of selenophene decreasing band gap resulted in red shift absorption. The onset values of wavelengths (λ_{onset}) were determined in order to calculate optical band gap (E_g^{op}) of polymers. The onset wavelengths were recorded as 664 nm and 636 nm for **P-SBTBDTT** and **P-TBTBDTT**, respectively. From the following equation, optical band gap values of **P-SBTBDTT** and **P-SBTBDTT** were obtained as 1.87 eV and 1.95 eV in sequence.

$$E_g^{op} = \frac{1241}{\lambda_{onset}}$$

As a result of electrochemical and spectroelectrochemical studies, optical band gap values of polymers were obtained lower in energy than their electronic band gap values caused by electron binding energy. The results of spectroelectrochemical studies were summarized in Table 2.

Table 2. Summary of Spectroelectrochemical Studies

	P-SBTBDTT	**P-TBTBDTT**
λ_{max} (nm)	540/590	519/561
E_g^{op} (eV)	1.87	1.95

Polaron and bipolaron bands formed on the spectra by oxidation with an external voltage. Polaron bands appeared in visible region while bipolaron bands formed in near infrared region. Absorbance intensity in neutral state decreased while absorption intensity of polaron and bipolaron bands increased as the oxidation potential

increased. **P-SBTBDTT** showed maximum absorbance at wavelengths around 790 nm and 1920 nm in Vis-NIR regions. On the other hand, **P-TBTBDTT** exhibited maximum absorption values at 780 nm and 1930 nm.

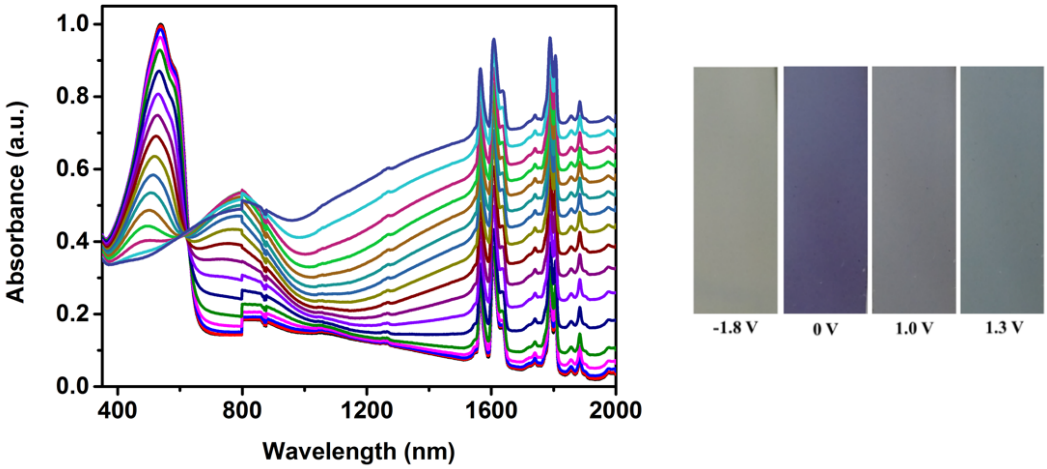

P-SBTBDTT

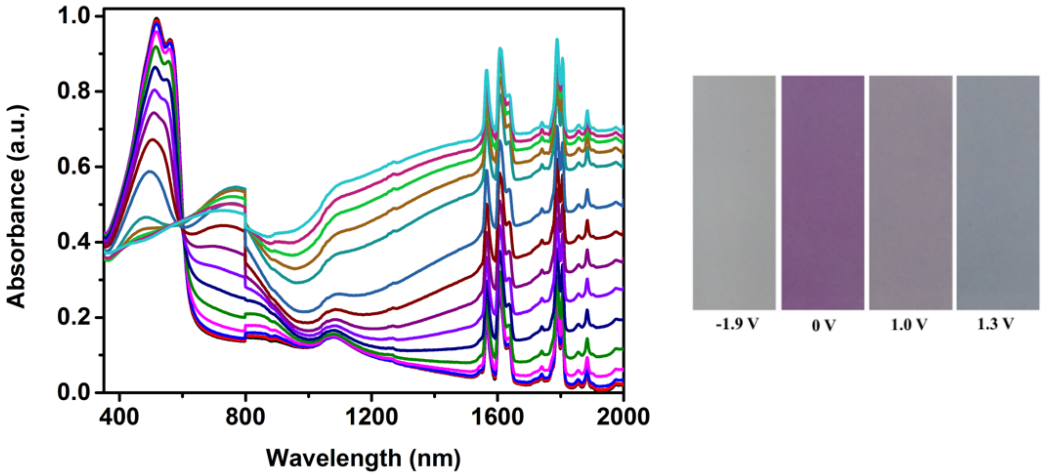

P-TBTBDTT

Figure 33. Electronic absorption spectra of polymers in 0.1 M $TBAPF_6$ / ACN electrolyte solution and the colors of corresponding polymers

Both of the polymers displayed broad absorption in visible region as shown in Figure 34. Polymers showed dual absorption peaks that could be ascribed to π-π^* transition and intermolecular charge transfer. The film states of both **P-SBTBDTT** and **P-SBTBDTT** showed red shifted absorption when compared to their chloroform solutions owing to more close-packed and ordered crystalline structures, aggregation and enhanced π-π stacking through polymer backbone due to increase in intermolecular interactions resulted in lower band gap.

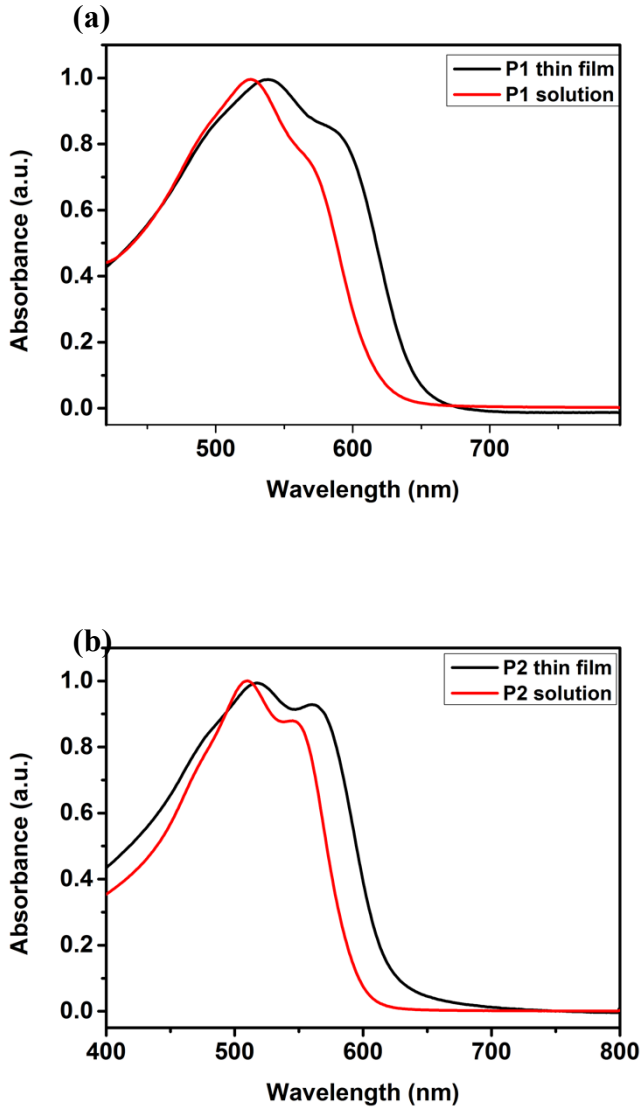

Figure 34. Absorption spectra of (a) **P-SBTBDTT**, (b) **P-TBTBDTT** in thin film and chloroform solution

3.3. Kinetic Studies

Chronoamperometric studies were conducted in order to monitor percent transmittance changes of polymers with respect to time and to observe their switching times at their maximum absorption wavelengths. Optical contrast and switching time values were determined by oxidation and reduction processes within 5 seconds time intervals for each cycle. Optical contrast values of **P-SBTBDTT** achieved as 35% (540 nm), 33% (790 nm) and 70% (1920 nm). Moreover, **P-TBTBDTT** showed optical contrast values of 29% (519 nm), 28% (780 nm) and 72% (1930 nm). Both of the polymers displayed high stability as shown in Figure 35. Switching times of **P-SBTBDTT** were recorded as 0.8 s (540 nm), 0.5 s (790 nm) and 1.2 s (1920 nm). On the other hand, **P-TBTBDTT** demonstrated switching times of 0.4 s (519 nm), 0.5 s (780 nm) and 0.5 s (1930 nm). The results of kinetic studies were summarized in Table 3.

Table 3. Summary of Kinetic Studies

	Optical contrast (ΔT %)		**Switching times (s)**
P-SBTBDTT	70	1920 nm	1.2
	33	790 nm	0.5
	35	540 nm	0.8
P-TBTBDTT	72	1930 nm	0.5
	28	780 nm	0.5
	29	519 nm	0.4

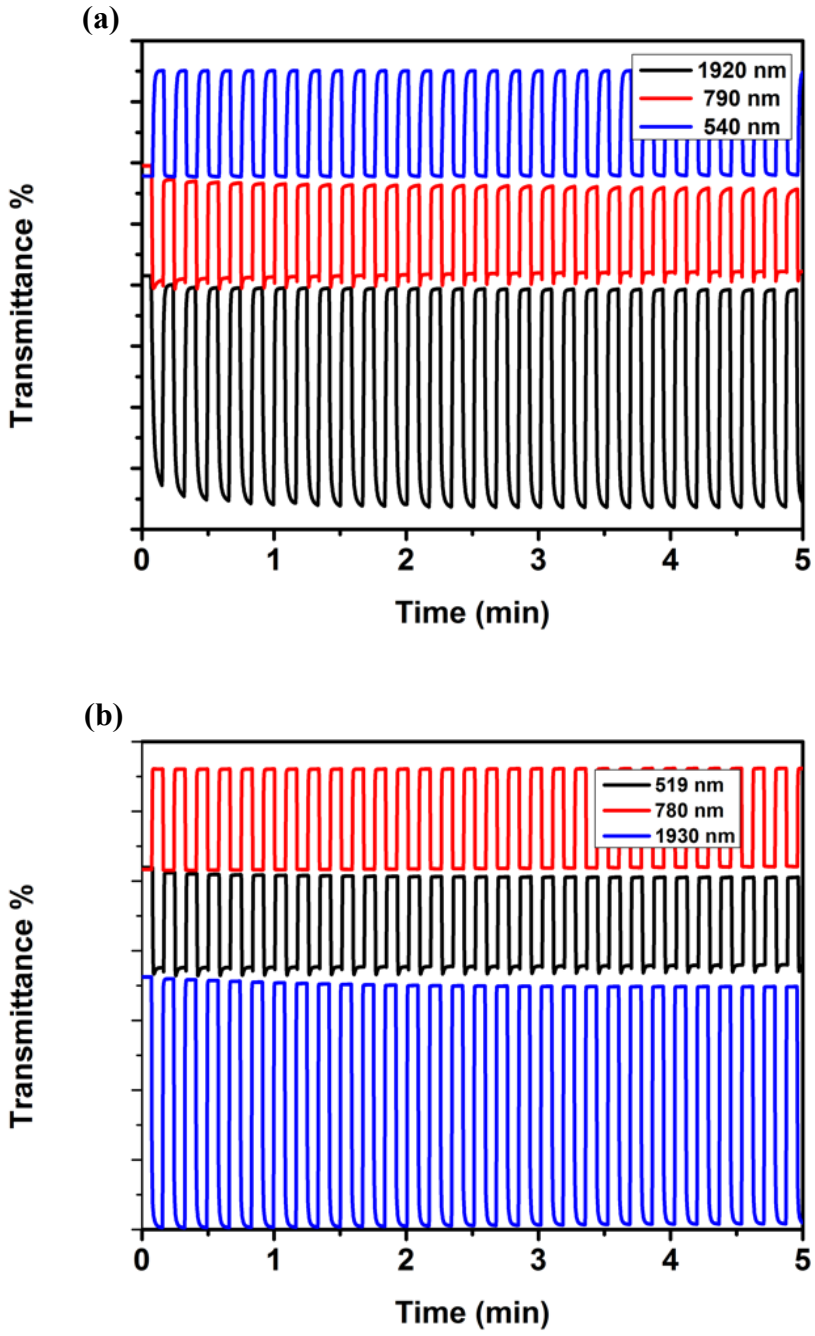

Figure 35. Percent transmittance change of (a) **P-SBTBDTT** (b) **P-TBTBDTT** in 0.1 M $TBAPF_6$ / ACN electrolyte solution at maximum wavelengths of polymers

3.4. Photovoltaic Studies

Electrochemical studies revealed that HOMO and LUMO energy levels and band gap of the polymers were applicable for photovoltaic studies. The energy levels of materials used in organic solar cell device fabrication were illustrated in Figure 36.

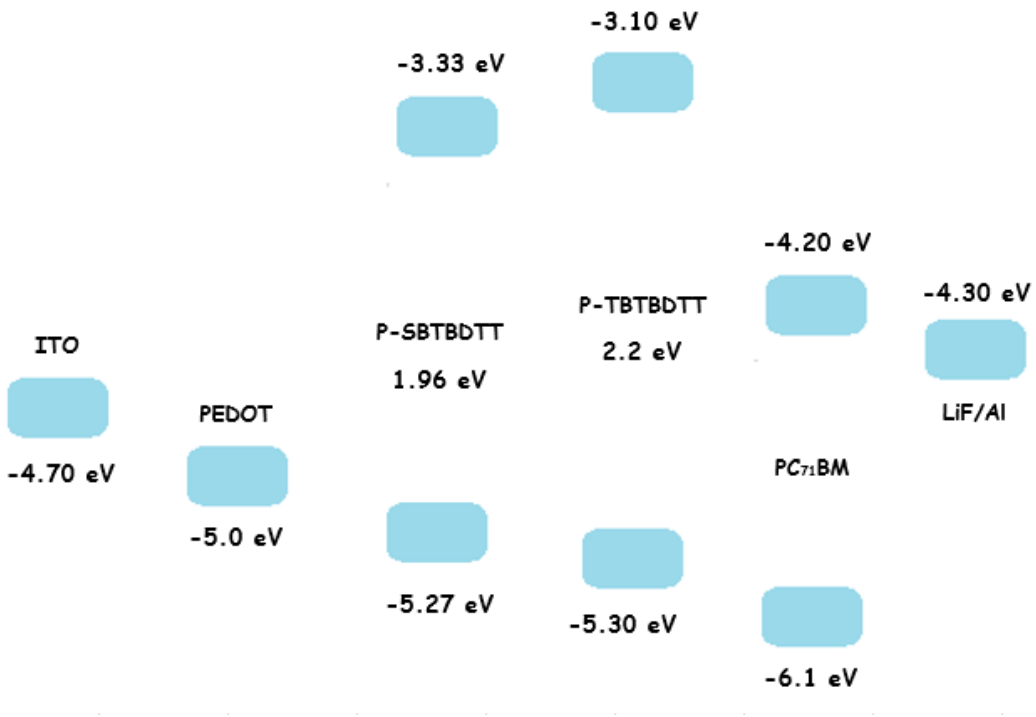

Figure 36. The energy levels of materials used in organic solar cell device fabrication

In a bulk heterojunction solar cell, synthesized polymers were used as donor materials in the active layer of device with the structure of ITO/PEDOT:PSS/Polymer:$PC_{71}BM$/LiF/Al. Polymer:PCBM ratio is a substantial parameter to obtain high power conversion efficiency (η) in solar cells. As PCBM amount increases electron transport also increases resulting in enhanced short circuit current and power conversion efficiency. On the other hand, if polymer amount decreases, collected photons decreases leading lowered short circuit current and power conversion efficiency. Therefore, polymer:PCBM ratio should be optimized. For this purpose, different ratios of polymer:PCBM layers were spin-coated on

PEDOT:PSS layers. LiF was used as charge collection layer in order to provide reduced energy barrier between the interface of active layer and Al cathode. Current density-voltage characteristics were studies under illumination of AM 1.5 G with 100 mW/cm^2. After obtaining current-voltage characteristics, power conversion efficiencies of polymers were calculated. Power conversion values of polymers could be affected by molecular weight, morphology, solvent and absorption in solar spectrum. In preliminary photovoltaic studies, the highest power conversion efficiency was obtained as 1.5% for **P-TBTBDTT**:$PC_{71}BM$ (1:2, w/w). On the other hand, the highest efficiency of **P-SBTBDTT**:$PC_{71}BM$ (1:2, w/w) was 1.2%. Theoretically, the difference between HOMO energy level of donor (polymer) and LUMO energy level of acceptor ($PC_{71}BM$) should give V_{OC} value. Experimentally, the V_{OC} values were obtained lower owing to high rate of recombination and energetic disorder. **P-TBTBDTT** showed the highest V_{OC} value of 0.72 V due to formation of charge transfer states between the acceptor fullerene (PCBM) and donor polymer. In addition, absorption, thickness and morphology were the factors affecting short circuit current. Although open-circuit voltage and short circuit current density values were moderately high, fill factor values were low ascribed to higher recombination of charge carriers than those of transportation and morphology. The best current density-voltage characteristics and the best photovoltaic results of polymers were obtained for polymer:PCBM ratio of 1:2, w/w which were demonstrated in Figure 37 and Table 4, respectively. In addition, the results of preliminary photovoltaic studies were summarized in Table 5.

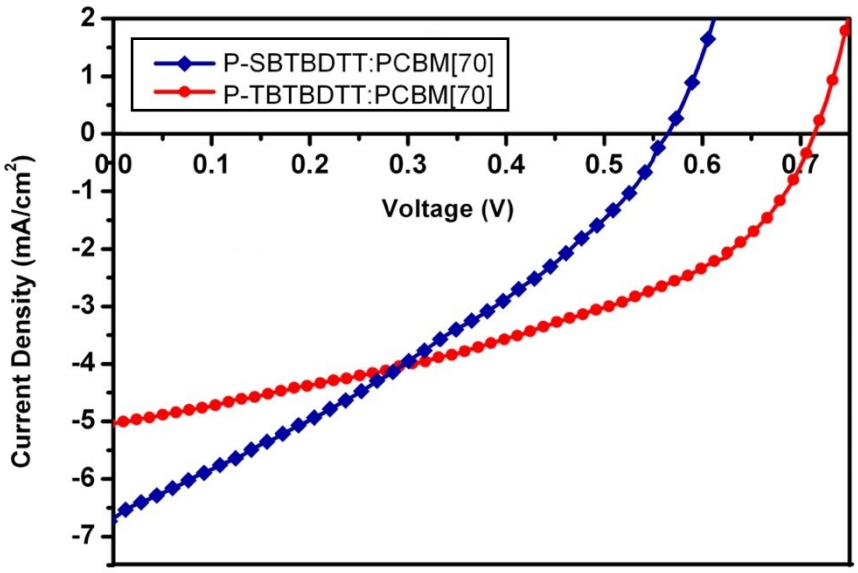

Figure 37. Current density-Voltage characteristics of polymer:PCBM (1:2, w/w)

Table 4. Summary of the best photovoltaic results of polymers

	V_{OC} (V)	J_{SC} (mA/cm^2)	V_{MP} (V)	I_{MP} (mA/cm^2)	FF (%)	η (%)
P-SBTBDTT	0.56	6.70	0.32	3.77	32	1.20
P-TBTBDTT	0.71	5.03	0.51	2.96	42	1.50

Table 5. Summary of Photovoltaic Studies

Polymer	Polymer $PC_{71}BM$ Ratio	V_{OC} (V)	J_{SC} (mA/cm^2)	FF (%)	η (%)
P-SBTBDTT	1:1	0.56	3.85	40	0.86
	1:2	0.56	6.70	32	1.20
	1:3	0.54	4.49	40	0.97
P-TBTBDTT	1:1	0.72	4.67	40	1.34
	1:2	0.71	5.03	42	1.50
	1:3	0.71	3.96	42	1.18

CHAPTER 4

CONCLUSIONS

In this study, conjugated polymers were synthesized for electrochemical and photovoltaic applications by donor-acceptor-donor approach. Stille coupling reactions were used to synthesize monomers and polymers. Electrochemical and optical properties of polymers were investigated. Furthermore, photovoltaic studies were performed by using polymers as active layers in bulk heterojunction solar cell devices.

In this research π-bridge donor moiety effects of selenophene and thiophene were investigated. Electrochemical studies revealed that polymers showed both n- and p-doping characters. Electronic band gap values were found as 1.96 eV and 2.2 eV for **P-SBTBDTT** and **P-TBTBDTT,** respectively. On the other hand, optical band gap values of **P-SBTBDTT** and **P-SBTBDTT** were obtained as 1.87 eV and 1.95 eV in sequence. As a result, optical band gap values of polymers were achieved lower than that of electronic band gaps owing to electron binding energy. In addition, selenophene based polymer **P-SBTBDTT** demonstrated lower band gap value with respect to thiophene based **P-TBTBDTT**. Furthermore, HOMO energy levels of **P-SBTBDTT** and **P-TBTBDTT** were calculated as -5.27 eV and -5.30 eV while LUMO energy levels were -3.33 eV and -3.10 eV, sequentially. Scan rate studies represented that redox processes of polymers were reversible and non-diffusion controlled. In spectroelectrochemical studies, polymers showed broad absorption in visible region. Polymer containing selenophene unit showed red shifted absorption when compared to thiophene analogue due to higher electron donating ability and quinoidal character of selenophene resulting in lower band gap. Moreover, the film states of polymers displayed red shifted absorption when compared to their chloroform solutions ascribed to more close-packed and ordered crystalline structure, intermolecular interactions enhanced by π-π stacking through polymer backbone,

aggregation and lower band gap of polymers in solid state. Kinetic studies showed that both of the polymers were highly stable with fast switching times. **P-TBTBDTT** displayed highest switching time of 0.4 s at 519 nm and highest optical contrast of 72% in NIR region.

Electrochemical and spectroelectrochemical studies indicated that both of the polymers were applicable for photovoltaic applications due to their proper band gaps, HOMO and LUMO energy levels and broad absorption ranges in visible region. As a consequence, polymers were used as donor materials in fabrication of bulk heterojunction solar cells. The organic solar cell device based on **P-TBTBDTT**:$PC_{71}BM$ (1:2, w/w) exhibited the best power conversion efficiency of 1.50% with a V_{oc} of 0.71 V, a J_{sc} of 5.03 mA/cm^2 and a FF of 42 %. In addition, **P-SBTBDTT**:$PC_{71}BM$ demonstrated its highest power conversion efficiency as 1.20% with 1:2, w/w having V_{oc} of 0.56 V, a J_{sc} of 6.70 mA/cm^2 and a FF of 32 %.

REFERENCES

1. Gowariker, V., & Viswanathan, N. (1986). *Polymer science*. New York: Wiley.

2. Macdiarmid, A. (2001). Synthetic metals: A novel role for organic polymers. *Synthetic Metals,* 11-22.

3. Chiang, C., Fincher, C., Park, Y., Heeger, A., Shirakawa, H., Louis, E., Macdiarmid, A. (1977). Electrical Conductivity in Doped Polyacetylene. *Physical Review Letters,* 1098-1101.

4. Friend, R., Gymer, R., Holmes, A., Burroughes, J., Marks, R., Taliani, C., Bradley, D., Dos Santos, D., Brédas, J., Lögdlund, M., Salaneck, W. (1999). Electroluminescence in conjugated polymers. *Nature, 397*, 121-128.

5. Beaujuge, P., & Reynolds, J. (2010). Color Control in π-Conjugated Organic Polymers for Use in Electrochromic Devices. *Chemical Reviews,* 268-320.

6. Horowitz, G. (1998). Organic Field-Effect Transistors. *Advanced Materials, 10*, 365-377.

7. Günes, S., Neugebauer, H., & Sariciftci, N. (2007). Conjugated Polymer-Based Organic Solar Cells. *Chemical Reviews,* 1324-1338.

8. Heller, A. (1990). Electrical wiring of redox enzymes. *Accounts of Chemical Research,* 128-134.

9. Pickup, P. (1990). Alternating current impedance study of a polypyrrole-based anion-exchange polymer. *Journal of the Chemical Society, Faraday Transactions, 86*, 3631.

10. Salzner, U., Lagowski, J., Pickup, P., & Poirier, R. (1998). Comparison of geometries and electronic structures of polyacetylene, polyborole, polycyclopentadiene, polypyrrole, polyfuran, polysilole, polyphosphole, polythiophene, polyselenophene and polytellurophene. *Synthetic Metals, 96*, 177-189.

11. Spanggaard, H., & Krebs, F. (2004). A brief history of the development of organic and polymeric photovoltaics. *Solar Energy Materials and Solar Cells, 83*, 125-146.

12. Heeger, A., Kivelson, S., Schrieffer, J., Su, P. (1988). Solutions in conducting polymers. *Rewievs of Modern Physics*, *60,* 781-851.

13. Skotheim, T. (1998). *Handbook of conducting polymers* (2nd ed.). New York: M. Dekker.

14. Potember, R., Hoffman, R., Hu, H., Cocchiaro, J., Viands, C., Murphy, R., & Poehler, T. (1987). Conducting organics and polymers for electronic and optical devices. *Polymer, 28*, 574-580.

15. Kumar, D., Sharma, R. (1998). Advances in conductive polymers. *European Polymer Journal, 34,* 1053-1060.

16. Chiang, C., Heeger, A., MacDiarmid, A. (1979). *Ber. Bunsenges. Phys. Chem.*, *83*, 407.

17. Nalwa, H., & Gazotti, W. (2001). Optical Devices Based on Conductive Polymers. In *Handbook of advanced electronic and photonic materials and devices*. Academic Press.

18. Roncali, J. (2007). Molecular Engineering of the Band Gap of π-Conjugated Systems: Facing Technological Applications. *Macromolecular Rapid Communications,* 1761-1775.

19. Bredas, J. (1985). Polarons, bipolarons, and solitons in conducting polymers. *Accounts of Chemical Research, 18*, 309-315.

20. Wudl, F., Kobayashi, M., Heeger, A. (1984). Poly(isothianaphthene). *The Journal of Organic Chemistry, 49,* 3382.

21. Ortí, E., Sanchís, M., Viruela, P., & Viruela, R. (1999). Effects of Carbon-sp^3 Bridging on the Electronic Properties of Oligothiophenes. *Synthetic Metals, 101,* 602-603.

22. Pei, Q., Zuccarello, G., Ahlskog, M., & Inganäs, O. (1994). Electrochromic and highly stable poly(3,4-ethylenedioxythiophene) switches between opaque blue-black and transparent sky blue. *Polymer, 35*, 1347-1351.

23. Cheng, Y., Yang, S., & Hsu, C. (2010). Synthesis of Conjugated Polymers for Organic Solar Cell Applications. *Chemical Reviews,* 5868-5923.

24. Kitamura, C., Tanaka, S., & Yamashita, Y. (1996). Design of Narrow-Bandgap Polymers. Syntheses and Properties of Monomers and Polymers Containing Aromatic-Donor and o -Quinoid-Acceptor Units. *Chemistry of Materials, 8*, 570-578.

25. Brocks, G., & Tol, A. (1996). Small Band Gap Semiconducting Polymers Made from Dye Molecules: Polysquaraines. *The Journal of Physical Chemistry, 100*, 1838-1846.

26. Yamamoto, T., Zhou, Z., Kanbara, T., Shimura, M., Kizu, K., Maruyama, T., Sasaki, S. (1996). π-Conjugated Donor−Acceptor Copolymers Constituted of π-Excessive and π-Deficient Arylene Units. Optical and Electrochemical Properties in Relation to CT Structure of the Polymer. *Journal of the American Chemical Society, 118*, 10389-10399.

27. Monk, P., & Mortimer, R. (1995). *Electrochromism: Fundamentals and applications*. Weinheim: VCH.

28. Mortimer, R. (1999). Organic electrochromic materials. *Electrochimica Acta, 44,* 2971-2981.

29. Argun, A., Aubert, P., Thompson, B., Schwendeman, I., Gaupp, C., Hwang, J., Reynolds, J. (2004). Multicolored Electrochromism in Polymers: Structures and Devices. *Chemistry of Materials, 16*, 4401-4412.

30. Berns, R., & Billmeyer, F. (2000). *Billmeyer and Saltzman's principles of color technology* (3rd ed.). New York: Wiley.

31. Sadki, S., Schottland, P., Brodie, N., & Sabouraud, G. (2000). The Mechanisms of Pyrrole Electropolymerization. *Chemical Society Reviews, 29*, 283-293.

32. Roncali, J. (1992). Conjugated poly(thiophenes): Synthesis, functionalization, and applications. *Chemical Reviews, 92*, 711-738.

33. Waltman, R., & Bargon, J. (1986). Electrically conducting polymers: A review of the electropolymerization reaction, of the effects of chemical structure on polymer film properties, and of applications towards technology. *Canadian Journal of Chemistry, 64*, 76-95.

34. Toshima, N., & Hara, S. (1995). Direct synthesis of conducting polymers from simple monomers. *Progress in Polymer Science, 20*, 155-183.

35. Cheng, Y., & Luh, T. (2004). Synthesizing optoelectronic heteroaromatic conjugated polymers by cross-coupling reactions. *Journal of Organometallic Chemistry, 689*, 4137-4148.

36. Tamao, K., Sumitani, K., & Kumada, M. (1972). Selective carbon-carbon bond formation by cross-coupling of Grignard reagents with organic halides. Catalysis by nickel-phosphine complexes. *Journal of the American Chemical Society, 94*, 4374-4376.

37. Miyaura, N., & Suzuki, A. (1995). Palladium-Catalyzed Cross-Coupling Reactions of Organoboron Compounds. *Chemical Reviews, 95*, 2457-2483.

38. Sonogashira, K. (2002). Development of Pd–Cu catalyzed cross-coupling of terminal acetylenes with sp2-carbon halides. *Journal of Organometallic Chemistry, 653*, 46-49.

39. Stille, J. (1986). The Palladium-Catalyzed Cross-Coupling Reactions of Organotin Reagents with Organic Electrophiles[New Synthetic Methods(58)]. *Angewandte Chemie International Edition in English, 25*, 508-524.

40. Thayer, A. (2005). Removing impurities. *Chemical & Engineering News, 83,* 55-58.

41. Hartwig, J. (2010). *Organotransition metal chemistry: From bonding to catalysis*. Sausalito, Calif.: University Science Books.

42. Tanimoto, A., & Yamamoto, T. (2004). Nickel-2,2′-Bipyridyl and Palladium-Triphenylphosphine Complex Promoted Synthesis of New π-Conjugated Poly(2-hexylbenzotriazole)s and Characterization of the Polymers. *Advanced Synthesis & Catalysis, 346*, 1818-1823.

43. Balan, A., Baran, D., Gunbas, G., Durmus, A., Ozyurt, F., & Toppare, L. (2009). One polymer for all: Benzotriazole containing donor–acceptor type polymer as a multi-purpose material. *Chemical Communications,* 6768-6770.

44. Gwinner, M., Brenner, T., Lee, J., Newby, C., Ober, C., Mcneill, C., & Sirringhaus, H. (2012). Organic field-effect transistors and solar cells using novel high electron-affinity conjugated copolymers based on alkylbenzotriazole and benzothiadiazole. *Journal of Materials Chemistry, 22*, 4436-4439.

45. Falzon, M., Wienk, M., & Janssen, R. (2011). Designing Acceptor Polymers for Organic Photovoltaic Devices. *The Journal of Physical Chemistry C, 115*, 3178-3187.

46. Sun, M., Niu, Q., Yang, R., Du, B., Liu, R., Yang, W., Cao, Y. (2007). Fluorene-based copolymers for color-stable blue light-emitting diodes. *European Polymer Journal, 43*, 1916-1922.

47. Chen, H., Hou, J., Zhang, S., Liang, Y., Yang, G., Yang, Y., Li, G. (2009). Polymer solar cells with enhanced open-circuit voltage and efficiency. *Nature Photonics, 3*, 649-653.

48. Liang, Y., Xu, Z., Xia, J., Tsai, S., Wu, Y., Li, G., Yu, L. (2010). For the Bright Future-Bulk Heterojunction Polymer Solar Cells with Power Conversion Efficiency of 7.4%. *Advanced Materials, 22*, E135-E138.

49. Chu, T., Lu, J., Beaupré, S., Zhang, Y., Pouliot, J., Wakim, S., Tao, Y. (2011). Bulk Heterojunction Solar Cells Using Thieno[3,4- c]pyrrole-4,6-dione and Dithieno[3,2- b :2′,3′- d]silole Copolymer with a Power Conversion Efficiency of 7.3%. *Journal of the American Chemical Society, 133*, 4250-4253.

50. Price, S., Stuart, A., Yang, L., Zhou, H., & You, W. (2011). Fluorine Substituted Conjugated Polymer of Medium Band Gap Yields 7% Efficiency in Polymer–Fullerene Solar Cells. *Journal of the American Chemical Society, 133*, 8057-8057.

51. Su, M., Kuo, C., Yuan, M., Jeng, U., Su, C., & Wei, K. (2011). Improving Device Efficiency of Polymer/Fullerene Bulk Heterojunction Solar Cells Through Enhanced Crystallinity and Reduced Grain Boundaries Induced by Solvent Additives. *Advanced Materials, 23*, 3315-3319.

52. Zhou, H., Yang, L., Stuart, A., Price, S., Liu, S., & You, W. (2011). Development of Fluorinated Benzothiadiazole as a Structural Unit for a Polymer Solar Cell of 7 % Efficiency. *Angewandte Chemie International Edition, 50*, 2995-2998.

53. Patra, A., & Bendikov, M. (2010). Polyselenophenes. *J. Mater. Chem., 20*, 422-433.

54. Das, S., & Zade, S. (2010). Poly(cyclopenta[c]selenophene): A new polyselenophene. *Chemical Communications, 46*, 1168-1168.

55. Patra, A., Wijsboom, Y., Leitus, G., & Bendikov, M. (2011). Tuning the Band Gap of Low-Band-Gap Polyselenophenes and Polythiophenes: The Effect of the Heteroatom. *Chemistry of Materials, 23*, 896-906.

56. Ha, J., Kim, K., & Choi, D. (2011). 2,5-Bis(2-octyldodecyl)pyrrolo[3,4- c]pyrrole-1,4-(2 H ,5 H)-dione-Based Donor–Acceptor Alternating Copolymer Bearing 5,5′-Di(thiophen-2-yl)-2,2′-biselenophene Exhibiting 1.5 cm 2 ·V −1 ·s −1 Hole Mobility in Thin-Film Transistors. *Journal of the American Chemical Society, 133*, 10364-10367.

57. Kroon, R., Lenes, M., Hummelen, J., Blom, P., & Boer, B. (2008). Small Bandgap Polymers for Organic Solar Cells (Polymer Material Development in the Last 5 Years). *Polymer Reviews, 48*, 531-582.

58. Młochowski, J., & Giurg, M. (2009). New Trends in Chemistry and Application of Aromatic and Related Selenaheterocycles. *Topics in Heterocyclic Chemistry Aromaticity in Heterocyclic Compounds,* 288-340.

59. Al-Hashimi, M., Han, Y., Smith, J., Bazzi, H., Alqaradawi, S., Watkins, S., Heeney, M. (2015). Influence of the heteroatom on the optoelectronic properties and transistor performance of soluble thiophene-, selenophene- and tellurophene–vinylene copolymers. *Chemical Science*.

60. Kularatne, R. S., Magurudeniya, H. D., Sista, P., Biewer, M. C., & Stefan, M. C. (2013). Donor-acceptor semiconducting polymers for organic solar cells. *Journal of Polymer Science Part A: Polymer Chemistry*, *51*(4), 743–768.

61. Gao, C., Wang, L., Li, X., & Wang, H. (2014). Rational design on D–A conjugated P(BDT–DTBT) polymers for polymer solar cells. *Polymer Chemistry, 5*, 5200-5210.

62. Sista, P., Biewer, M., & Stefan, M. (2011). Benzo[1,2-b:4,5-b′]dithiophene Building Block for the Synthesis of Semiconducting Polymers. *Macromolecular Rapid Communications, 33*, 9-20.

63. Sista, P., Kularatne, R., Mulholland, M., Wilson, M., Holmes, N., Zhou, X., Stefan, M. (2013). Synthesis and photovoltaic performance of donor-acceptor polymers containing benzo[1,2- b :4,5- b ′]dithiophene with thienyl substituents. *Journal of Polymer Science Part A: Polymer Chemistry, 51*, 2622-2630.

64. Beaujuge, P., & Reynolds, J. (2010). Color Control in π-Conjugated Organic Polymers for Use in Electrochromic Devices. *Chemical Reviews, 110*, 268-320.

65. Içli-Özkut, M., Mersini, J., Önal, A., & Cihaner, A. (2011). Substituent and heteroatom effects on the electrochromic properties of similar systems. *Journal of Polymer Science Part A: Polymer Chemistry, 50*, 615-621.

66. Osken, I., Bildirir, H., & Ozturk, T. (2011). Electrochromic behavior of poly(3,5-bis(4-bromophenyl)dithieno[3,2-b;2′,3′-d]thiophene). *Thin Solid Films, 519*, 7707-7711.

67. Usluer, O., Koyuncu, S., Demic, S., & Janssen, R. (2010). A novel high-contrast ratio electrochromic material from spiro[cyclododecane-1,9′-fluorene]bicarbazole. *Journal of Polymer Science Part B: Polymer Physics, 49*, 333-341.

68. Kumar, A., Welsh, D., Morvant, M., Piroux, F., Abboud, K., & Reynolds, J. (1998). Conducting Poly(3,4-alkylenedioxythiophene) Derivatives as Fast Electrochromics with High-Contrast Ratios. *Chemistry of Materials, 10*, 896-902.

69. Sonmez, G., Schottland, P., Zong, K., & Reynolds, J. (2001). Highly transmissive and conductive poly[(3,4alkylenedioxy)pyrrole2,5diyl] (PXDOP) films prepared by air or transition metal catalyzed chemical oxidation. *Journal of Materials Chemistry, 11*, 289-294.

70. Rosseinsky, D., & Mortimer, R. (2001). Electrochromic Systems and the Prospects for Devices. *Advanced Materials, 13*, 783-793.

71. Xu, C., Liu, L., Legenski, S., Ning, D., & Taya, M. (2004). Switchable window based on electrochromic polymers. *Journal of Materials Research, 19*, 2072-2080.

72. Monk, P., Delage, F., & Vieira, S. (2001). Electrochromic paper: Utility of electrochromes incorporated in paper. *Electrochimica Acta, 46*, 2195-2202.

73. Burroughes, J. H., Bradley, D. D. C., Brown, A. R., Marks, R. N., Mackay, K., Friend, R. H., Holmes, A. B. (1990). Light-emitting diodes based on conjugated polymers. *Nature*, *347*(6293), 539–541.

74. Stutzmann, N. (2003). Self-Aligned, Vertical-Channel, Polymer Field-Effect Transistors. *Science, 29*, 1881-1884.

75. Ling, Q., Chang, F., Song, Y., Zhu, C., Liaw, D., Chan, D., Neoh, K. (2006). Synthesis and Dynamic Random Access Memory Behavior of a Functional Polyimide. *Journal of the American Chemical Society, 128*, 8732-8733.

76. Thompson, B., & Fréchet, J. (2008). Polymer–Fullerene Composite Solar Cells. *Angewandte Chemie International Edition, 47*, 58-77.

77. Hoppe, H., & Sariciftci, N. (2004). Organic solar cells: An overview. *Journal of Materials Research, 19*, 1924-1945.

78. Zhou, X., Blochwitz, J., Pfeiffer, M., Nollau, A., Fritz, T., & Leo, K. (2001). Enhanced Hole Injection into Amorphous Hole-Transport Layers of Organic Light-Emitting Diodes Using Controlled p-Type Doping. *Advanced Functional Materials, 11*, 310-314.

79. Gregg, B. (2003). Excitonic Solar Cells. *The Journal of Physical Chemistry B, 107*, 4688-4698.

80. Qi, B., & Wang, J. (2012). Open-circuit voltage in organic solar cells. *Journal of Materials Chemistry, 22*, 24315-24325.

81. Brabec, C., Cravino, A., Meissner, D., Sariciftci, N., Fromherz, T., Rispens, M., Hummelen, J. (2001). Origin of the Open Circuit Voltage of Plastic Solar Cells. *Advanced Functional Materials, 11*, 374-380.

82. Scharber, M., Mühlbacher, D., Koppe, M., Denk, P., Waldauf, C., Heeger, A., & Brabec, C. (2006). Design Rules for Donors in Bulk-Heterojunction Solar Cells—Towards 10 % Energy-Conversion Efficiency. *Advanced Materials, 18*, 789-794.

83. Liu, J., Shi, Y., & Yang, Y. (2001). Solvation-Induced Morphology Effects on the Performance of Polymer-Based Photovoltaic Devices. *Advanced Functional Materials, 11*, 420.

84. Brabec, C., Shaheen, S., Winder, C., Sariciftci, N., & Denk, P. (2002). Effect of LiF/metal electrodes on the performance of plastic solar cells. *Applied Physics Letters, 80*, 1288.

85. Hung, L., Tang, C., & Mason, M. (1997). Enhanced electron injection in organic electroluminescence devices using an Al/LiF electrode. *Applied Physics Letters, 70*, 152.

86. Jabbour, G., Kawabe, Y., Shaheen, S., Wang, J., Morrell, M., Kippelen, B., & Peyghambarian, N. (1997). Highly efficient and bright organic electroluminescent devices with an aluminum cathode. *Applied Physics Letters, 71*, 1762.

87. Padilla, M., Michl, B., Thaidigsmann, B., Warta, W., & Schubert, M. (2014). Short-circuit current density mapping for solar cells. *Solar Energy Materials and Solar Cells, 120*, 282-288.

88. Qi, B., & Wang, J. (2013). Fill factor in organic solar cells. *Physical Chemistry Chemical Physics, 15*, 8972-8982.

89. Schilinsky, P. (2004). Simulation of light intensity dependent current characteristics of polymer solar cells. *Journal of Applied Physics, 95*, 2816.

90. Riedel, I., & Dyakonov, V. (2004). Influence of electronic transport properties of polymer-fullerene blends on the performance of bulk heterojunction photovoltaic devices. *Physica Status Solidi (a), 201*, 1332-1341.

91. Maennig, B., Drechsel, J., Gebeyehu, D., Simon, P., Kozlowski, F., Werner, A., Parisi, J. (2004). Organic p-i-n solar cells. *Applied Physics A: Materials Science and Processing*, *79*, 1–14.

92. Unay, H., Unlu, N., Hizalan, G., Hacioglu, S., Yildiz, D., Toppare, L., & Cirpan, A. (2014). Benzotriazole and benzodithiophene containing medium band gap polymer for bulk heterojunction polymer solar cell applications. *Journal of Polymer Science Part A: Polymer Chemistry, 53*, 528-535.

93. Lee, J., Kim, J., Moon, B., Kim, H., Kim, M., Shin, J., Cho, K. (2015). Two-Dimensionally Extended π-Conjugation of Donor–Acceptor Copolymers via Oligothienyl Side Chains for Efficient Polymer Solar Cells. *Macromolecules, 48*, 1723-1735.

94. Zhang, S., Ye, L., Zhao, W., Liu, D., Yao, H., & Hou, J. (2014). Side Chain Selection for Designing Highly Efficient Photovoltaic Polymers with 2D-Conjugated Structure. *Macromolecules, 47*(14), 4653-4659.

95. Yin, N., Wang, L., Ma, Y., Lin, Y., Wu, J., Luo, Q., Zhao, X. (2015). 4,8-Bis(thienyl)-benzo[1,2-b:4,5-b′]dithiophene based A-π-D-π-A typed conjugated small molecules with mono-thiophene as the π-bridge: Synthesis, properties and photovoltaic performance. *Dyes and Pigments, 120*, 299-306.

96. Pilgram, K., Zupan, M., & Skiles, R. (1970). Bromination of 2,1,3-benzothiadiazoles. *Journal of Heterocyclic Chemistry, 7*(3), 629-633.

97. Tsubata, Y., Suzuki, T., Miyashi, T., & Yamashita, Y. (1992). Single-component organic conductors based on neutral radicals containing the pyrazino-TCNQ skeleton. *The Journal of Organic Chemistry, 57*(25), 6749-6755.

98. Pinhey, J. T., & Roche, E. G. (1988). The chemistry of organolead(IV) tricarboxylates. Synthesis and electrophilic heteroarylation reactions of 2- and 3-thienyl-, and 2- and 3-furyl-lead tricarboxylates. *Journal of the Chemical Society, Perkin Transactions 1,* (8), 2415.

99. Ellinger, S., Ziener, U., Thewalt, U., Landfester, K., & Möller, M. (2007). Synthesis and Self-Organization of α,ω-Substituted Oligothiophenes with Long, Branched Alkyl Substituents. *Chemistry of Materials, 19*(5), 1070-1075.

100. Erlik, O., Unlu, N. A., Hizalan, G., Hacioglu, S. O., Comez, S., Yildiz, E. D., Toppare, L., Cirpan, A. (2015). Silafluorene-based polymers for electrochromic and polymer solar cell applications. *Journal of Polymer Science Part A: Polymer Chemistry, 53*(13), 1541-1547.

APPENDIX A

NMR DATA

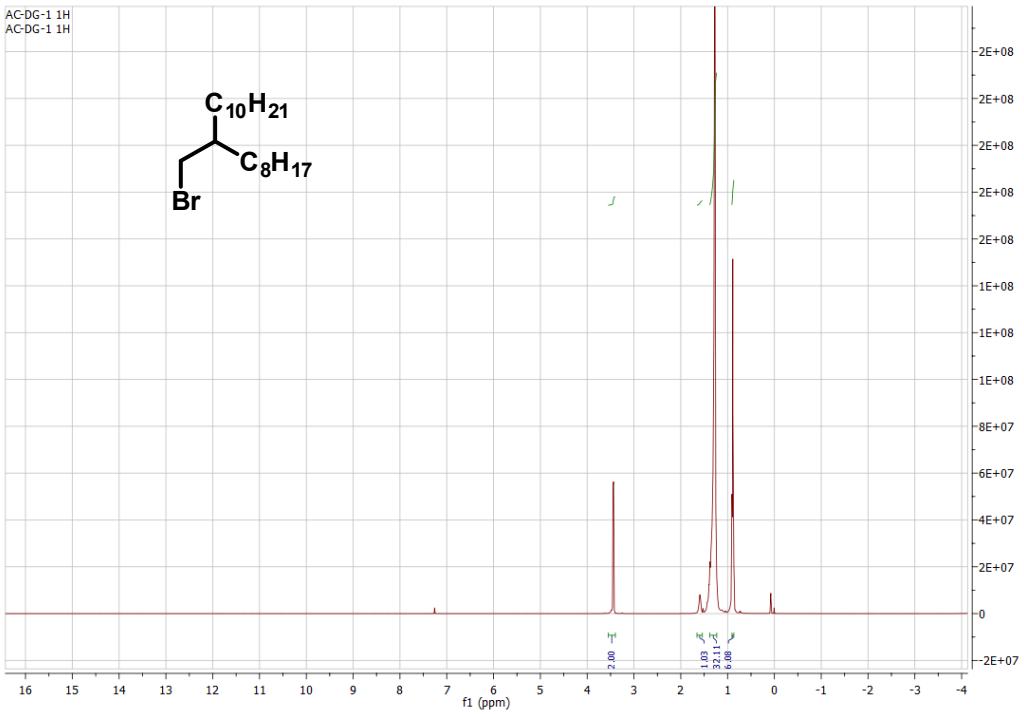

Figure 38. ^{1}H NMR result of 9-(bromomethyl)nonadecane

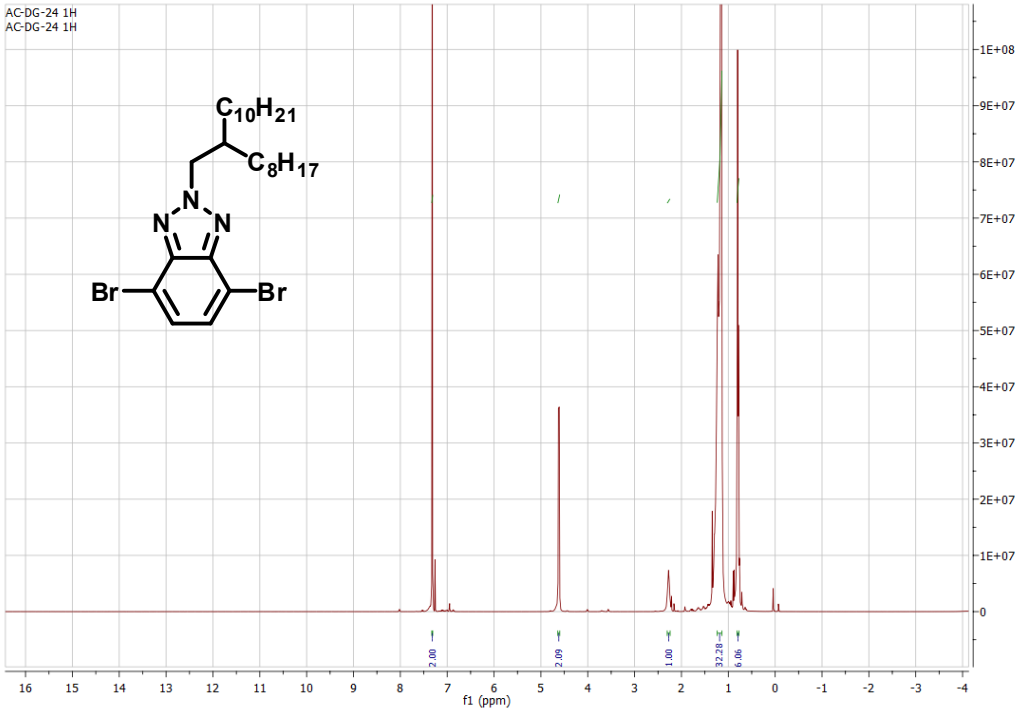

Figure 39. ^{1}H NMR result of 4,7-dibromo-2-(2-octyldodecyl)-2H-benzo[d][1,2,3]triazole

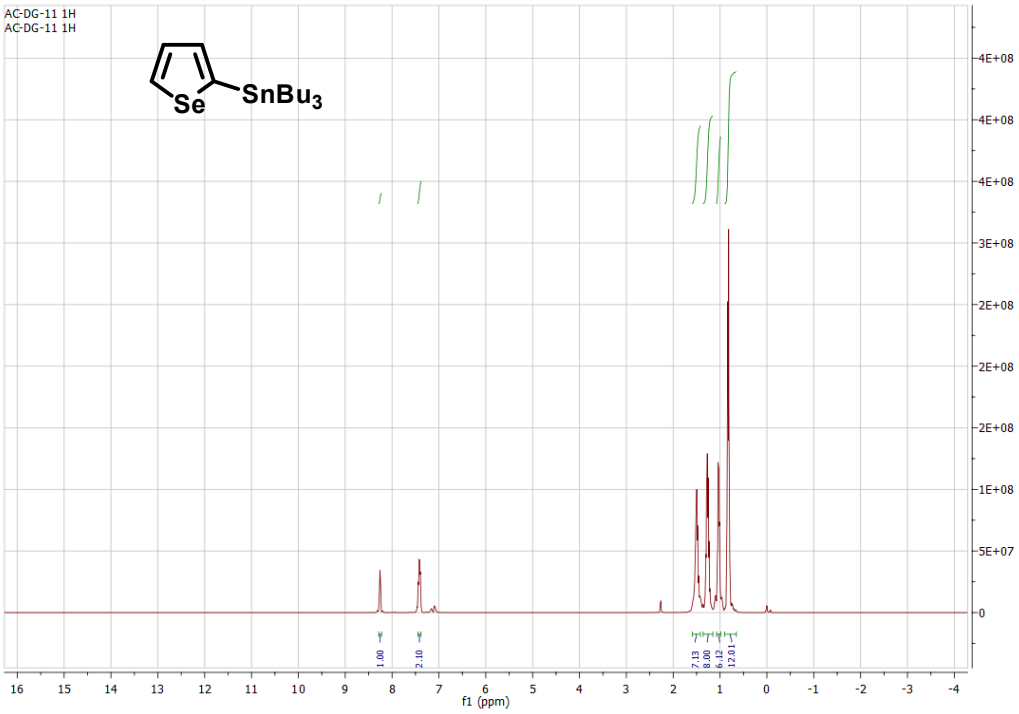

Figure 40. ^{1}H NMR result of of Tributyl(selenophen-2-yl)stannane

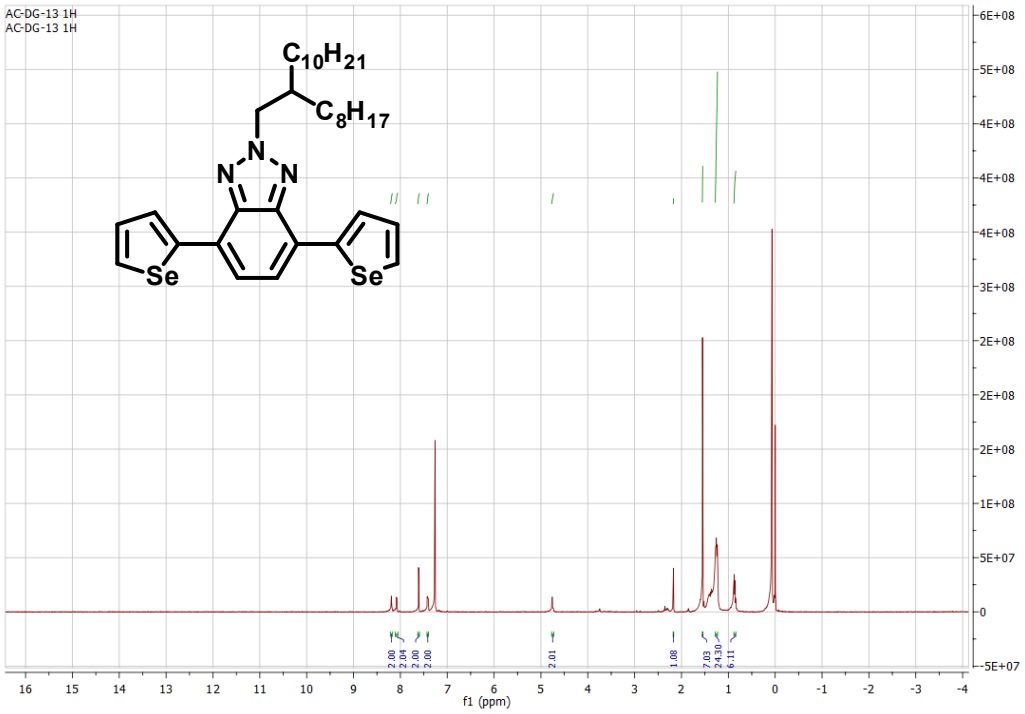

Figure 41. [1]H NMR result of 2-(2-octyldodecyl)-4,7-di(selenophen-2-yl)-2H-benzo[d][1,2,3]triazole

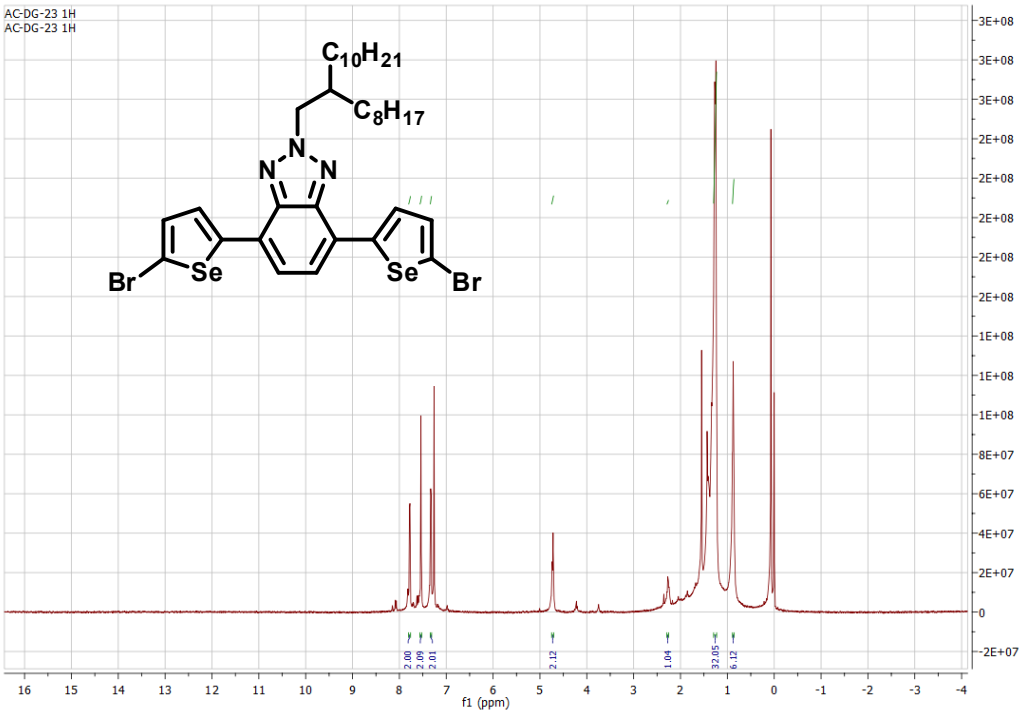

Figure 42. ^{1}H NMR result of 4,7-bis(5-bromoselenophen-2-yl)-2-(2-octyldodecyl)-2H-benzo[d][1,2,3]triazole

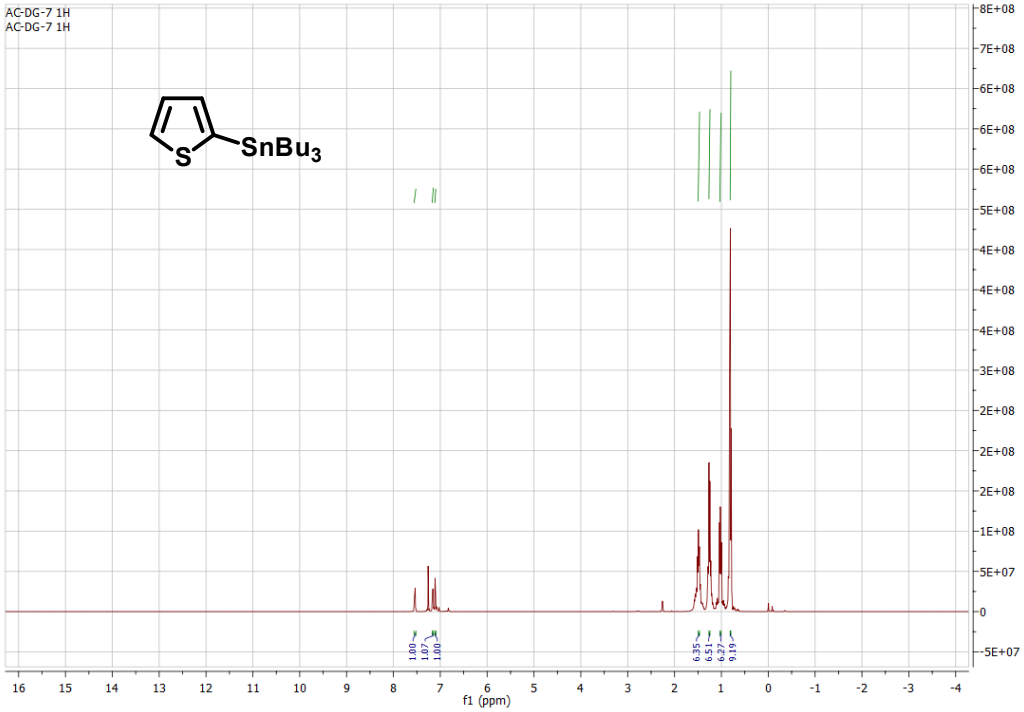

Figure 43. ^{1}H NMR result of Tributyl(thiophen-2-yl)stannane

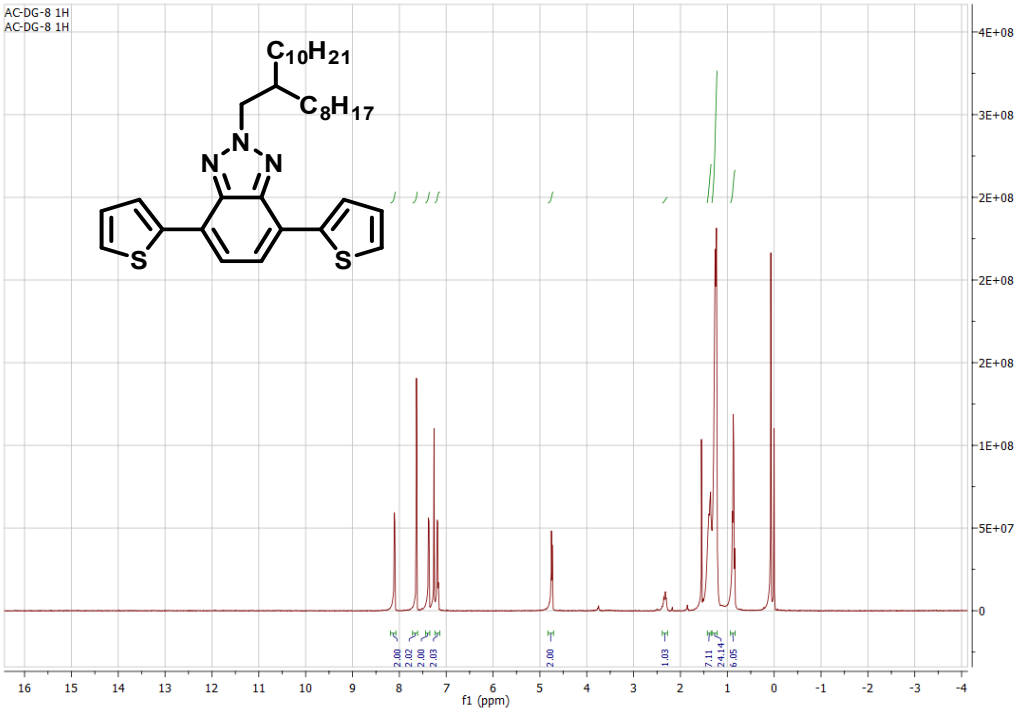

Figure 44. [1]H NMR result of 2-dodecyl-4,7-di(thiophen-2-yl)-2H-benzo[d][1,2,3]triazole

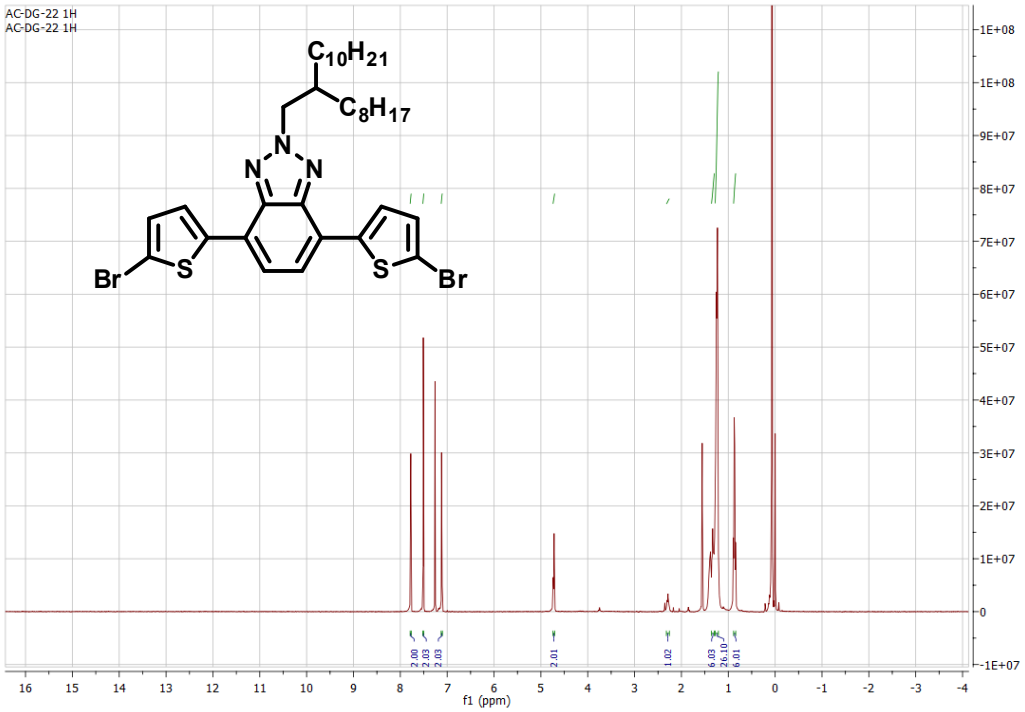

Figure 45. ^{1}H NMR result of 4,7-bis(5-bromothiophen-2-yl)-2-(2-octyldodecyl)-2H-benzo[d][1,2,3]triazole

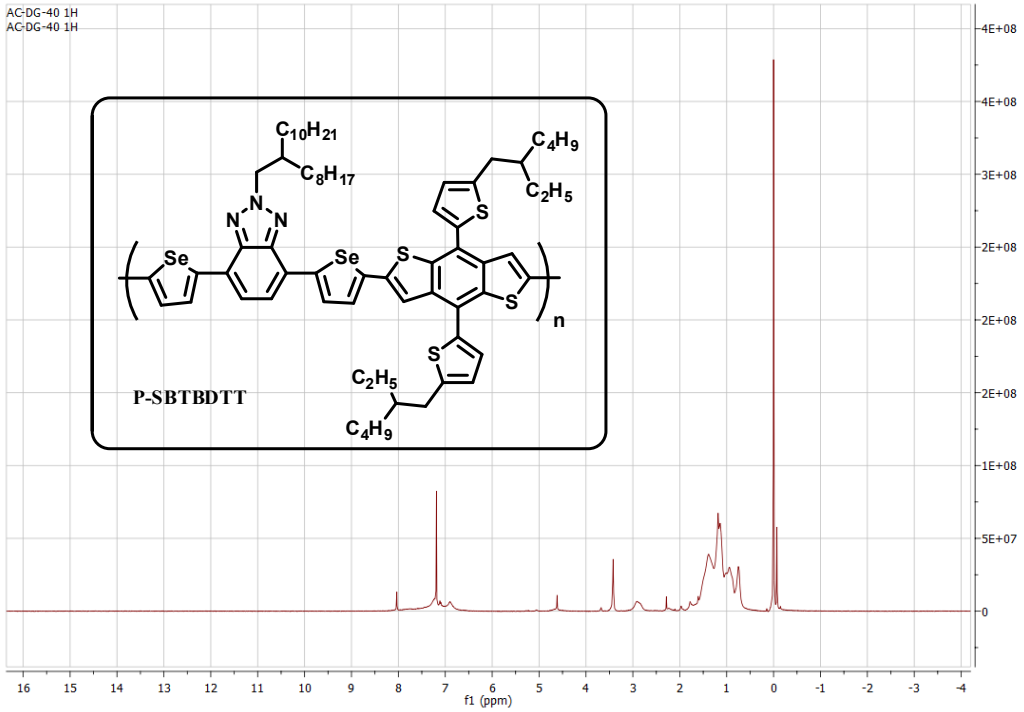

Figure 46. ^{1}H NMR result of **P-SBTBDTT**

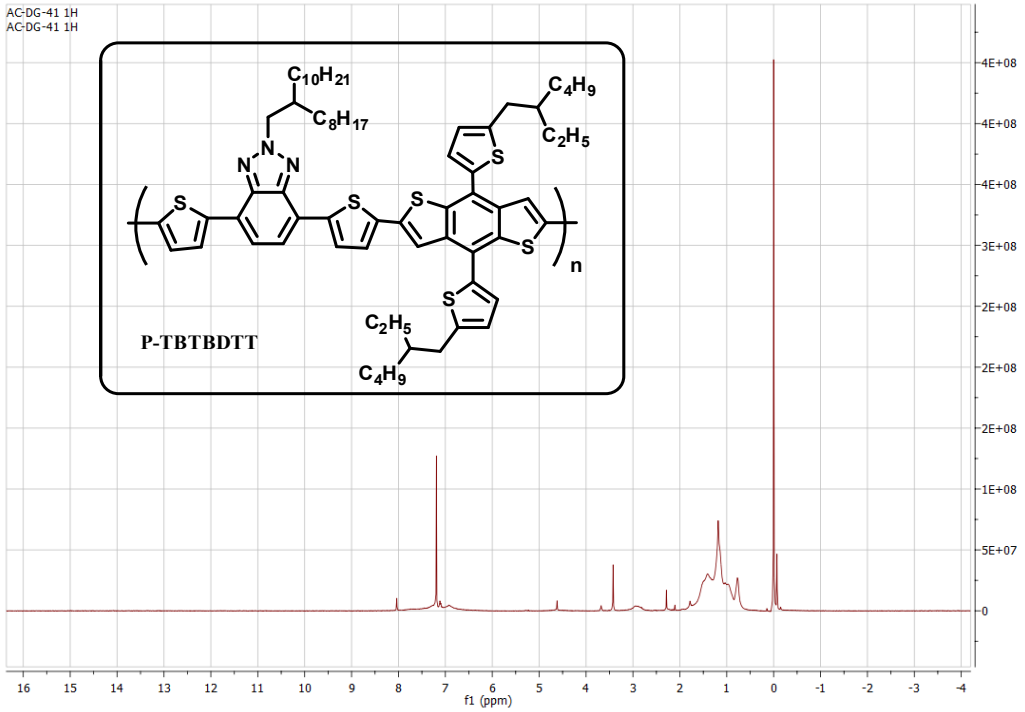

Figure 47. 1H NMR result of **P-TBTBDTT**